Journal of Soft Computing in Civil Engineering 5-3 (2021) 101-133

Contents lists available at SCCE

Journal of Soft Computing in Civil Engineering

Journal homepage: www.jsoftcivil.com

Damage Localization of RC Beams via Wavelet Analysis of Noise Contaminated Modal Curvatures

H. Jahangir[1], H. Hasani[2], M.R. Esfahani[3*]

1. Assistant Professor, Department of Civil Engineering, University of Birjand, Birjand, Iran
2. M.Sc. Student, Department of Civil Engineering, University of Birjand, Birjand, Iran
3. Professor, Department of Civil Engineering, Faculty of Engineering, Ferdowsi University of Mashhad, Mashhad, Iran

Corresponding author: *esfahani@um.ac.ir*

https://doi.org/10.22115/SCCE.2021.292279.1340

ARTICLE INFO

Article history:
Received: 26 June 2021
Revised: 20 September 2021
Accepted: 29 October 2021

Keywords:
Damage location;
Wavelet transform;
Noisy contaminated condition;
Modal curvature;
RC beams.

ABSTRACT

In this paper, the location of single, double, and triple damage scenarios in reinforced concrete (RC) beams are assessed using the Wavelet transform coefficient. To achieve this goal, the numerical models of RC concrete beams were conducted based on the experimental specimens. The mode shapes and corresponding modal curvatures of the RC beam models in damaged and undamaged status were considered as input signals in Wavelet transform. By considering the Wavelet coefficient as damage index, Daubechies, Biorthogonal, and Reverse Biorthogonal Wavelet families were compared to select the most proper one to identify damage locations. Moreover, various sampling distances and their influence on the damage index were studied. In order to simulate the practical situations, two kinds of noises were added to modal data and then denoised by Wavelet analysis to check the proposed damage index in noisy conditions. The results revealed that among the wavelet families, rbio2.4 and rbio2.2 outperform others in detecting damage locations using mode shapes and modal curvatures, respectively. As expected, the sensitivity of modal curvatures to different damage scenarios is more the mode shapes. By increasing sampling distances from 25 mm to 100 mm, the accuracy of the proposed damage index reduces. In order to eliminate boundary effects, it is necessary to use windowing techniques. Applying Wavelet denoising methods on noise-contaminated modal curvatures leads to proper damage localization in both types of noises.

How to cite this article: Jahangir H, Hasani H, Esfahani MR. Damage localization of RC beams via wavelet analysis of noise contaminated modal curvatures. J Soft Comput Civ Eng 2021;5(3):101–133. https://doi.org/10.22115/scce.2021.292279.1340.

1. Introduction

Reinforced concrete (RC) structures [1–3] and consequently their elements such as RC columns, slabs and beam are classified as important in maintenance point of view [3,4]. Therefore, detection of initial cracks and damages in these structural elements cause future maintenance and repair costs [5,6]. Early structural damage detection is one of the first steps in structural rehabilitation [7–11] and strengthening [12–15]. Among different damage detection techniques, vibrational based damage detection is a regular and prominent one which consists of detecting how changes in the structure, such as stiffness loss, cause changes in its dynamics characteristics, such as natural frequencies, mode shapes, and modal damping, named modal data [16–18]. The literature recommends a variety of approaches for identifying structural damage using modal data [19–22]. In his analysis of damage detection methods, Salawu [23] found that frequency changes were effective in most circumstances, although mode shapes were also necessary. It has been shown by Pandey et al. [24] that the absolute change in mode shape curving can be used as an effective damage indicator since it is much more sensitive to damage than mode shapes. According to Dawari and Vesmawala [25], the method of modal curvature (second derivative of mode shape) and the modal flexibility method were used to detect cracking in reinforced concrete beams. In particular, mode shapes are often used to detect damages, since they contain local data about the damage and are highly resistant to environmental influences [26,27]. But, noise can easily contaminate damage induced uniqueness in mode shapes, and it only gets shown at unreasonably high damage levels [28]. Elimination of noise from mode shapes needs effective soft computing methods [29–32] or signal processing techniques such as wavelet transforms. The simultaneous ability of reducing noises and detecting minor singularities in mode shapes, caused many researcher to utilize different Wavelet mothers such as Mexican hat [33]. Gabor [34], Haar [35] and Debauchies [36] in structural damage detection field. Zhu et al. [37] utilized Wavelet transform in order to identify damages in functionally graded beams. An index calculating the location of damage is calculated based on the maximum wavelet coefficients in the scale field; this index is known as the damage index. As described in Table 1, several researchers used wavelets as damage detection techniques and consider modal data of damaged and undamaged structure as input signals.

Table 1
The tabulated damage detection related studies.

Reference	Year	Type of studied structure	Method
[38]	2012	Steel Beams	Wavelet / Frequencies
[39]	2013	Steel Plates	Wavelet / Deflections
[40]	2014	General Analytical Beam	Wavelet Finite Element / Support Vector Regression
[41]	2016	General Analytical Beam	Complex Wavelet / Modal Curvature
[42]	2021	Concrete Beam	Wavelet / Time History Domain
[43]	2021	Concrete Beam	Wavelet / Vibrational Based Responses
[44]	2021	Pre-stressed Concrete Slab	Contourlet / Mode Shapes

2. Research significance

Reviewing previous studies in wavelet based damage detection field reveals that, although there are various kinds of mother wavelets with different properties, up to now, none of them is introduces as the most proper and unique one in detecting structural damages. On the other hand, RC structural elements such as RC beams play an important role in construction industry and their failure cause catastrophic financial and life detriments. Moreover, just limited research works investigate the influence of noises in modal based damage detection methods. Therefore, in this paper, an experimental RC beam reported in previous study of one of the authors of this paper is considered as the basis of conducting numerical finite element model. Then, single, double and triple damage scenarios were created by reducing the stiffness in some specific areas of the numerical model. The mode shape and modal curvatures of the damaged and undamaged models were introduced to wavelet transform as input signals and the resulted wavelet coefficient were utilized to identify damage scenarios. After comparison of different mother wavelets, the most suitable wavelet for detection of locations of the damage scenarios is selected. Moreover, the effect of sampling distances on the results of wavelet transform is investigated. After selection of suitable wavelet and considering the degrees of freedom with the distance of 100 mm, the hypothesis testing method was used for locating the damage scenarios. In addition, in order to have more consistency with the data and environmental conditions, which happen in practice, two kind of noises were added to mode shapes of numerical specimens. Then the noise was eliminated from the modal data by adopting the deniosing techniques using wavelets; and ability of the index resulted from hypothesis testing was tested for locating the damages in noisy data. As defined in Ibrahim [45], the soft computing techniques are computational methods deal with approximate models and gives solutions to complex real-life problems, which is completely related to the core goal of the paper in deniosing process, as a complex problem by approximately dividing the high and low frequency parts of the signals, which could not be done without using computers.

3. Method

3.1. Wavelet transform

In order to conduct signal processing, it is possible to use wavelets, as a kind of transforms, to generate variable size windows. Such transformation has been enhanced with regard to local changes by focusing on short time intervals for high frequency components and focusing on lengthy periods for low-frequency components [46]. Instead of using frequency, the wavelets transform uses an inverse proportional scale. As a result of wavelet transformation, an input collection of functions is divided into waves, each associated with a wavelet called Mother Wavelet, $\psi(x)$ [47]. The function $\psi(t,a,b)$ is the scaled and translated mother wavelet in wavelet transformation:

$$\psi(t,s,b)=\frac{1}{\sqrt{s}}\psi\left(\frac{t-b}{s}\right) \tag{1}$$

Within Eq. (1), s and b represent scale and translation, respectively. Parameterizing the wavelet transformation is scaling and translating its coefficients. The scaling of a wavelet refers to its compression or stretching. However, translating a wavelet means that its start has been delayed [47].

Continuous wavelet transform (CWT) means the whole amount of the signal multiplied by the wavelet function scaled and translated $\psi(t, a, b)$:

$$CWT(s,b) = \int_{-\infty}^{\infty} f(t) \cdot \psi(t,s,b) dt \tag{2}$$

The wavelet coefficients of the scale and position functions are provided by Eq. (2). The coefficients illustrate how the wavelet function relates to the original signal and how similar it is. As the coefficients increase, the wavelet's form and result will become more similar. Coefficients of calculation generate a large amount of data at any scale. Using dyadic scales and positions, the analysis data is reduced by making use of the power of two (known as dyadic scales and positions). This kind of analysis is known as Discrete Wavelet Transform (DWT). As a result of Mallat's study [46], filter analysis is called fast transformation wavelets today. The wavelet coefficient could be the output of this toolbox in which the input is the original signal. The wavelet function is defined as follows during this transformation:

$$\psi_{j,k}(t) = \frac{1}{\sqrt{2^j}} \psi\left(\frac{t - 2^j k}{2^j}\right) = 2^{-j/2} \psi(2^{-j} t - k) \tag{3}$$

Eq. (3) gives j as the decomposition level, t as the time, and $2j$ as the scale. According to Eq. (4), the discrete wavelet transformation coefficients are calculated by multiplying the *f(t)* signal by the translated and scaled wavelet $\psi_{j,k}(t)$:

$$DWT(j,k) = \int_{-\infty}^{\infty} f(t) \cdot \psi_{j,k}(t) dt \tag{4}$$

During the discrete wavelet transform, the original signal passes through high-pass and low-pass filters. Filters are time-independent linear operators. Using a low-pass filter, bumps in a signal are smoothed out. With a high-pass filter, bumps in the signal are displayed and smooth regions are eliminated or reduced [19]. Approximation coefficients are considered high-scale low-frequency components of a signal and high-scale components are referred to as detail coefficients. Using the wavelet, the original signal can be filtered in order to identify such components. Decomposition of the approximation coefficients in sequence might continue the process. As a result of this method, a large number of components are separated into the original signal, called the decomposition tree. The decomposing wavelet tree has vital data. This tree provides access to the signal approximation and detail coefficients at each level. The input signal used to identify damage consists of abrupt and high frequency damage to a building.

The discrete wavelet transform (DWT) uses both the wavelet function $\psi(t)$ and the scaling function $\emptyset(x)$, as opposed to the continuous wavelet transform (CWT) method that only employs the wavelet function. The low-pass filter is associated with wavelet functions, and the high-pass

filter with scaling functions. The scaling feature works in a similar way to wavelet. In fact, wavelet coefficients are detailed, and scaling coefficients produce an approximation of the original signal. Among the wavelet functions, only the orthogonal wavelet has a scaling function [48].

There are multiple families of wavelets that have been introduced for signal processing and they may be categorized based on their various properties [46]. Among the wavelet families Gaussian, Mexican, Shannon, and Morlet, there are no wavelet properties specific to them ψ, Their squatting function is not present $\emptyset$, They are therefore incapable of converting discrete wavelets, and therefore cannot be rebuilt using discretion. Wavelet analysis consists of transforming a constant wavelet. In summary, Haar, Daubechies, and Coiflet waves do not exhibit a strong relationship ψ. Due to the presence of the scaling function $\emptyset$, the discrete wavelet function can also be used within these wavelets. They are slightly regular and not symmetrical. Another type of wavelets that are symmetri quely and precisely reconstructable of wavelets is the Biorthogonal wavelets and the opposite way around, the Reverse Biorthogonal wavelets. In addition, they feature two types of wavelet and scaling functions.

Wavelets and signal properties determine which wavelet is best suited to process the signal of a certain phenomenon. In most cases, it can be difficult to know for sure which wavelet is appropriate for use and that was determined by tried and error. In this study, many mother waves are used to identify damage using the family of Daubechies, Biorthogonals, and Reverse Biorthogonals wavelets.

3.2. Experimental specimens

As an experimental reference to assess the ability of proposed damage detection method in practical applications, as presented in Fig. 1, a reinforced concrete (RC) beams named B1 with 150 mm width, 200 mm height and 2200 mm length which vibrational modal tests are conducted on them by Baghiee et al. [49] were selected. Table 1 describes the geometrical and mechanical properties of the RC beam [49]. As presented in Fig. 2, In order to obtain vibrational data, modal tests were conducted in a suspended position to reduce the effect of supports and the noise resulted by random vibrations of the floor. In these tests, the degrees of freedom were considered on central axis on the upper face of the sample with a 100 mm distance from each other [49].

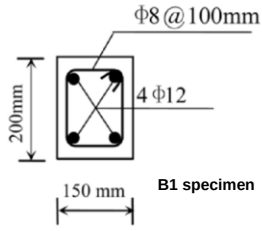

Fig. 1. The cross-section of the experimental specimens (B1) [49].

Table 1
The geometrical and mechanical properties of experimental specimens [49].

Specimen	f'_{cu} (MPa)	A'_s (mm^2)	A'_s (mm^2)	stirrup distance (mm)	d (mm)	d' (mm)
B1	20	226	226	100	175	25

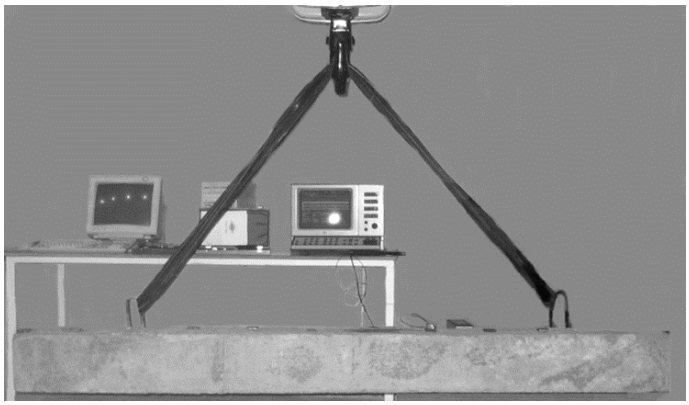

Fig. 2. Suspended beams in vibration test.

In conducted modal tests, the frequency response functions (FRFs) were resulted by measuring the excitation force and responses of specimens in time field and their projection in frequency field. In order to determine the fundamental modal parameters including natural frequencies and mode shapes, the mathematical curve fitting techniques were analyzed using STAR Program. Fig. 3 shows the mode shapes of B1 specimen. The experimental mode shapes were normalized relative to their greatest vibration amplitude [49].

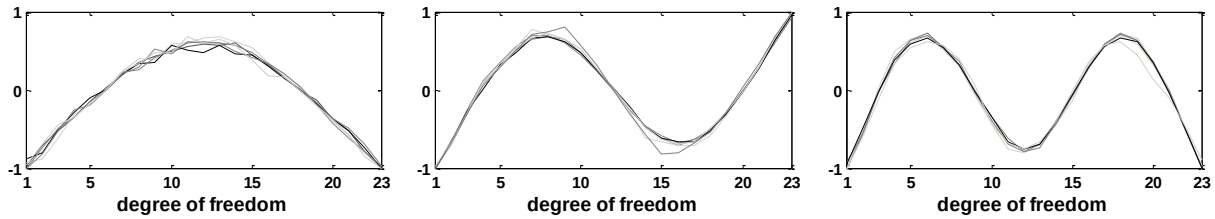

Fig. 3. Mode shapes of the experimental specimen B1: a) mode 1; b) mode 2 and c) mode 3 [49].

3.3. Verification of numerical model

As the damage scenarios are studied in numerical models, the 2D numerical model of the undamaged experimental B1 specimen were developed by ABAQUS [50] finite element software. This model includes 528 plane tension 2D elements (CPE4R) for concrete and 308 truss 2D elements (T2D2) for steel bars. Fig. 4 shows the numerical model of the concrete beam specimen. The degrees of freedom were considered with distances of 100 mm from each other to be in accordance with experimental specimens. The properties of concrete and steel used in this model are provided in Table 2.

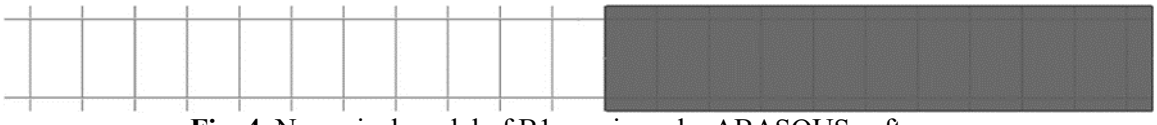

Fig. 4. Numerical model of B1 specimen by ABASQUS software.

Table 2
Mechanical properties of the materials in the numerical model.

Material	Elasticity Coefficient (GPa)	Density (kg/m^3)	Poisson Ratio	f_{cu} (Mpa)	f_y (Mpa)
Concrete	17	2400	0.17	20	---
Steel	200	7850	0.3	---	400

In this numerical analysis the boundary conditions were considered same as the test of suspended status and frequencies of numerical analysis and experimental method were so close together; which can be seen in Table 3. Fig. 5 show the comparison of experimental and numerical mode shapes. According to Fig. 5, the experimental data and numerical data are in good agreement with each other.

Table 3
Experimental and numerical natural frequencies of B1 specimen.

Mode Number	Special Frequencies (Hz)	
	FEM Analyze	Experimental Results
First Mode	114.28	114.28
Second Mode	298.42	304.89
Third Mode	560.24	563.19

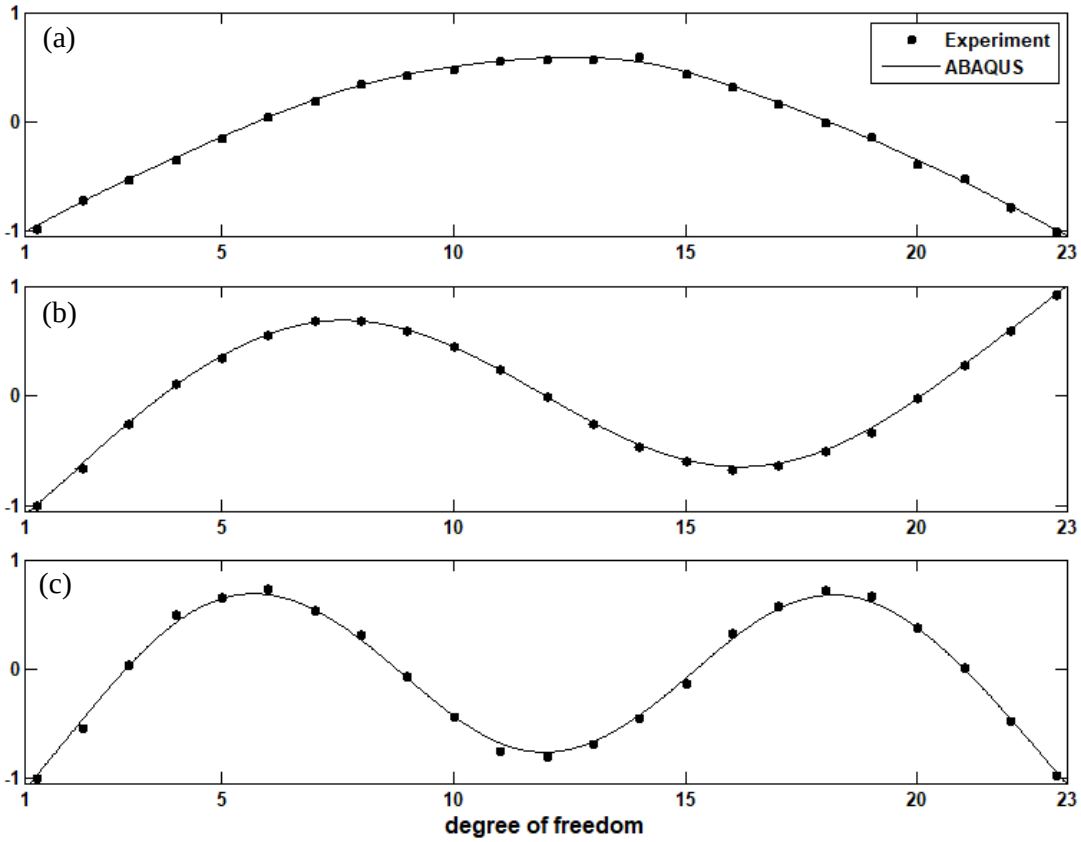

Fig. 5. Mode shapes of numerical and experimental of B1 specimen: a) First Mode; b) Second Mode and c) Third Mode.

3.4. Damage scenarios

In this paper, some damage scenarios were developed in the numerical model to test abilities of the damage detecting methods. These single, double and triple damage scenarios were as reduction in elastic modulus of concrete in some parts of the beam. The location and percentage of concrete elastic modulus reduction for these damages are represented in Table 4 and Fig. 6.

Table 4
Properties of damage scenarios in numerical models.

Damages Scenario	Types of Damage	Percentage Reduction of Concrete	Damage Location (***x***) (mm)
D1	Single Damage	40	1100
D2	Double Damage	20	600 and 1600
D3	Triple Damage	20	600, 1200 and 1600

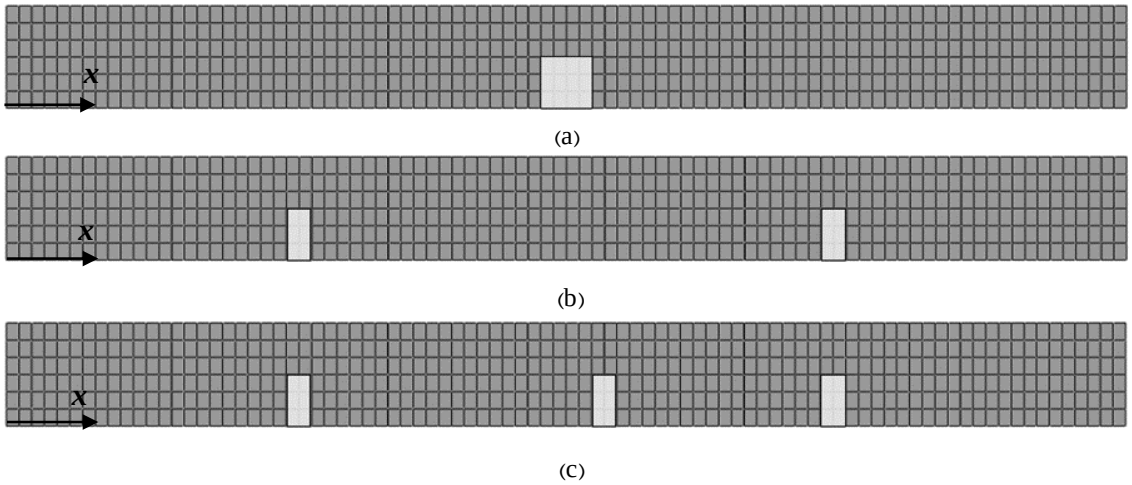

Fig. 6. Locations of different damage scenarios: L_1, L_2 and L_3.

3.5. Best mother wavelet and sampling distance

Before evaluating the ability of wavelet based damage detecting methods and using various damage indices that can be defined for them, it is required to choose best mother wavelet for analyzing the received signals from the structure. The quality of selecting the optimized and suitable wavelet for signal processing depends on the properties of the wavelet and the signal. In most cases one wavelet could not be used with absolute certainty and this procedure should be done through trial and error. In this paper, mother wavelets were chosen by considering the first mode shape of specimen in single damage scenario state as the input signal. Also the degrees of freedom were set with distances of 25 mm, 50 mm, 75 mm and 100 mm from each other in order to evaluate the effectiveness of sampling distances on the proposed method.

The signals of vibrational mode shape and its corresponding modal curvature (second derivation of mode shape) obtained by using central difference approximation were calculated after curve fitting with spline functions. Fig. 7 demonstrates the first mode shape and corresponding modal curvature of specimen in single damage scenario status (D1).

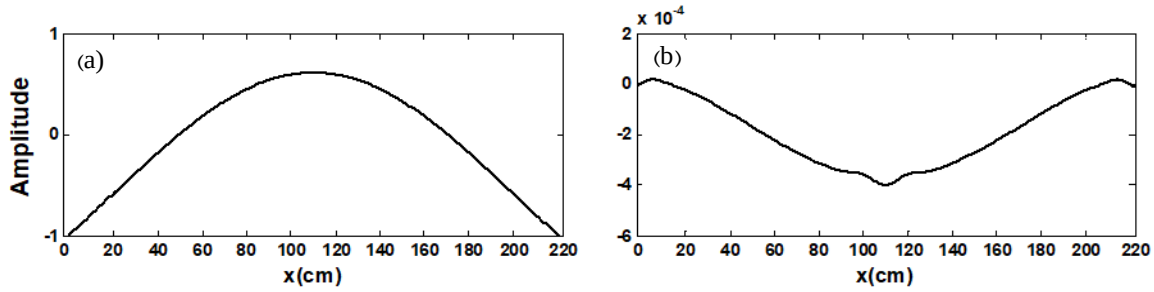

Fig. 7. a) The first mode shape and b) modal curvature of the specimen in single damage scenario (D1).

As it could be seen in Fig. 7, there is no significant change in mode shape in the location of damage. This change is negligible in the case of modal strain too. Therefore, identification of damage location demands more process of modal data via best wavelet transform and choosing optimal sampling distance.

Initial investigations show that among different wavelets, bior2.4 and bior3.5 from Biorthogonal wavelet family, db2 and db3 from Daubechies family and rbio2.2, rbio2.4 and rbio3.3 from Reverse Biorthogonal family are more sensitive to location of damages compared to other wavelets. Figs. 8, 9 and 10 show wavelet functions ($\psi(x)$) and scale of ($\phi(x)$) of these families.

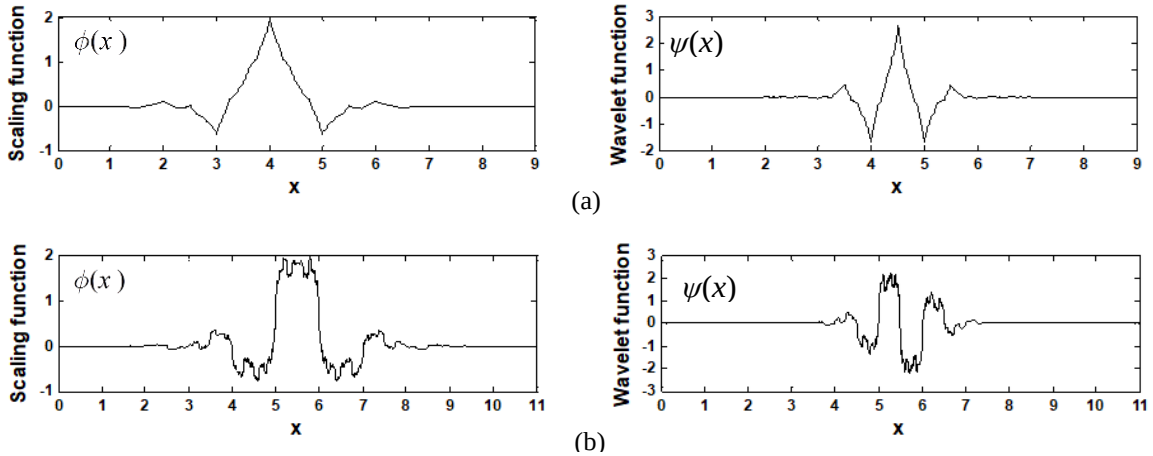

Fig. 8. Biorthogonal wavelet family: a) bior2.4 and b) bior3.5 [51].

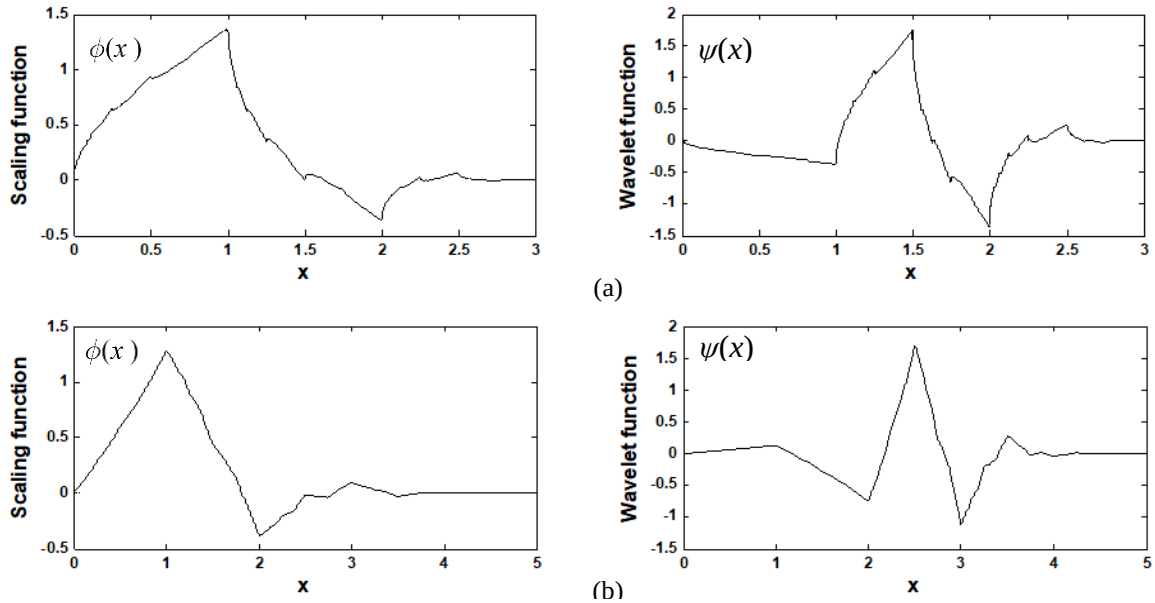

Fig. 9. Daubechies wavelet family: a) db2 and b) db3 [51].

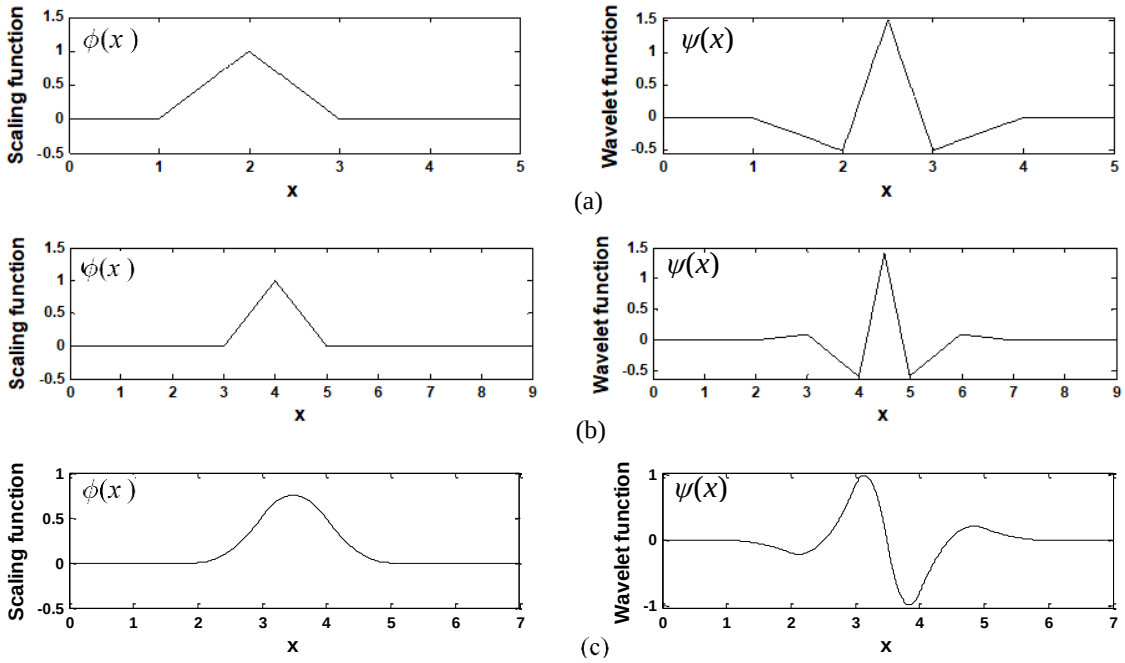

Fig. 10. Reverse Biorthogonal wavelet family: a) rbio 2.2; b) rbio 2.4 and c) rbior 3.3 [51].

Studies on the results of these wavelets for single damage scenario show that details signal obtained from wavelet transform of the first mode shape and modal curvature by use of bior2.4 and db2 have similar behavior to that of rbio2.2. This behavior similarity in different sampling distances can be seen in Figs. 11 and 12, respectively.

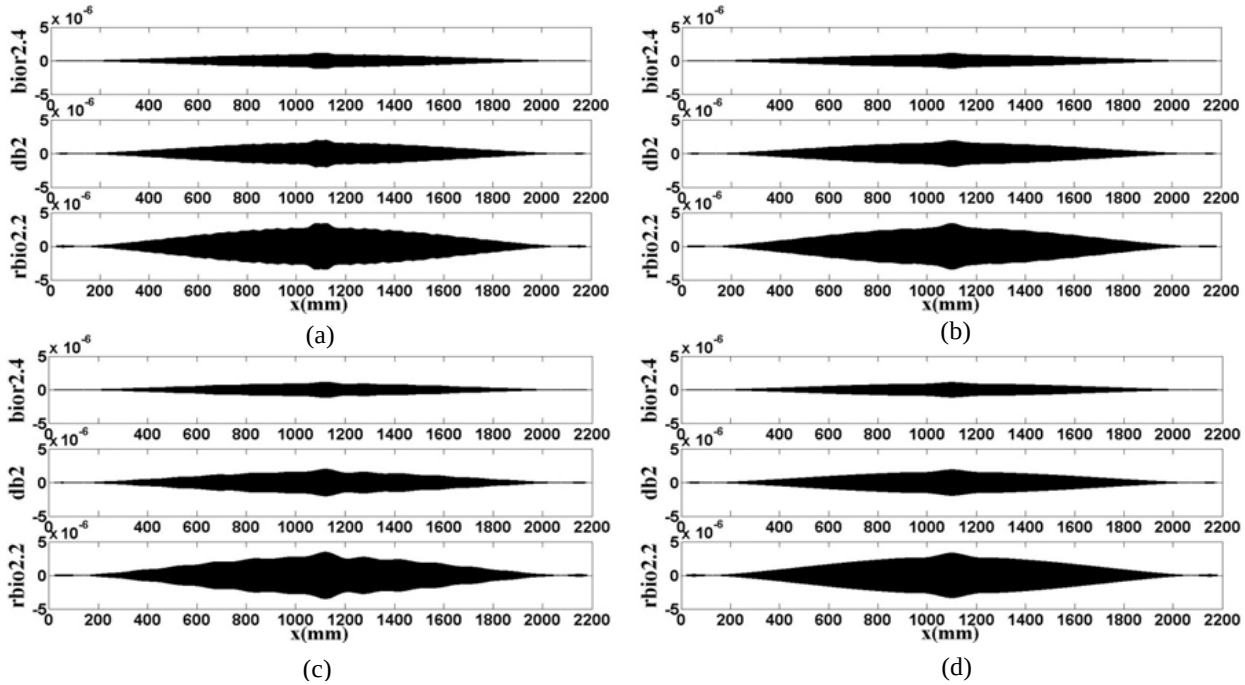

Fig. 11. Details signal of the first mode shape using bior2.4, db2 and rbio2.2 wavelets at sampling distance of: a) 25 mm; b) 50 mm; c) 75 mm and d) 100 mm.

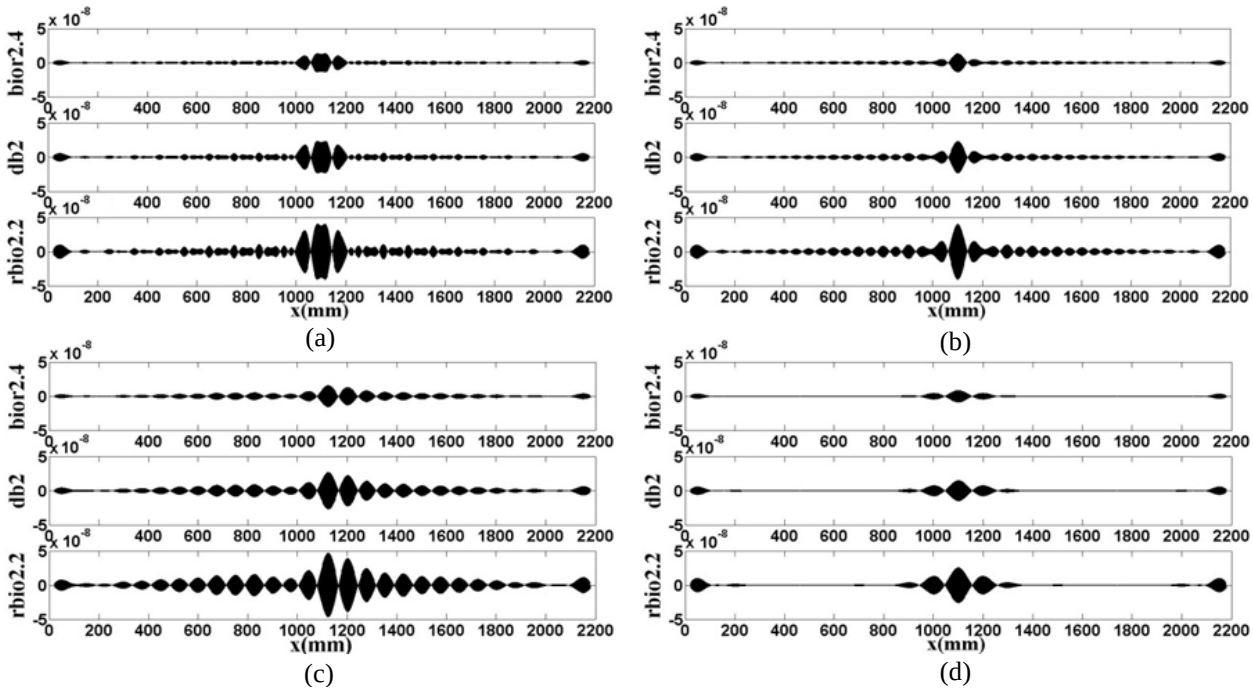

Fig. 12. Details signal of the first modal curvature using bior2.4, db2 and rbio2.2 wavelets at sampling distance of: a) 25 mm; b) 50 mm; c) 75 mm and d) 100 mm.

As it shown in Fig. 11, the signals of details calculated using rbio2.2 mother wavelet has a greater amplitude than db2 and bior2.4. In addition, maximum range of these signals estimate damage location to some extent and increasing the sampling distance will reduce the ability of the method. Fig. 12 shows the detail signals resulted from rbio2.2 mother wavelet on the first modal curvature also have a greater range than bior2.4 and db2. Moreover, location of damage has appeared better by the detail signals obtained from modal curvature. The error developed in sampling distance of 75 mm can be assumed to be caused by symmetry of some mother wavelets and asymmetry of these distances. Comparing detail signals obtained from application of bior2.4, db2 and rbio2.2 mother wavelets on the first mode shape and modal curvature, it can be concluded that due to similar behavior and greater amplitudes of wavelet rbio2.2 than the two other wavelets, rbio2.2 wavelet can be utilized instead of both bior2.4 and db2.

The studies indicate that detail signals resulted from wavelets bior3.5 and db3 have a similar behavior to that of wavelet rbio3.3. Figs. 13 and 14 show this similar behavior for the first mode shape and modal curvature in the four sampling distances, respectively. Figs. 13 and 14 show that for both of first mode shape and modal curvature, the detail signals calculated using mother wavelet rbio3.3 have greater amplitudes compared to bior3.5 and db3. In different sampling distances, locating damage scenario by using modal curvature is more accurate in comparison with mode shape. Hence, rbio3.3wavelet can be employed as a replace for the two other wavelets.

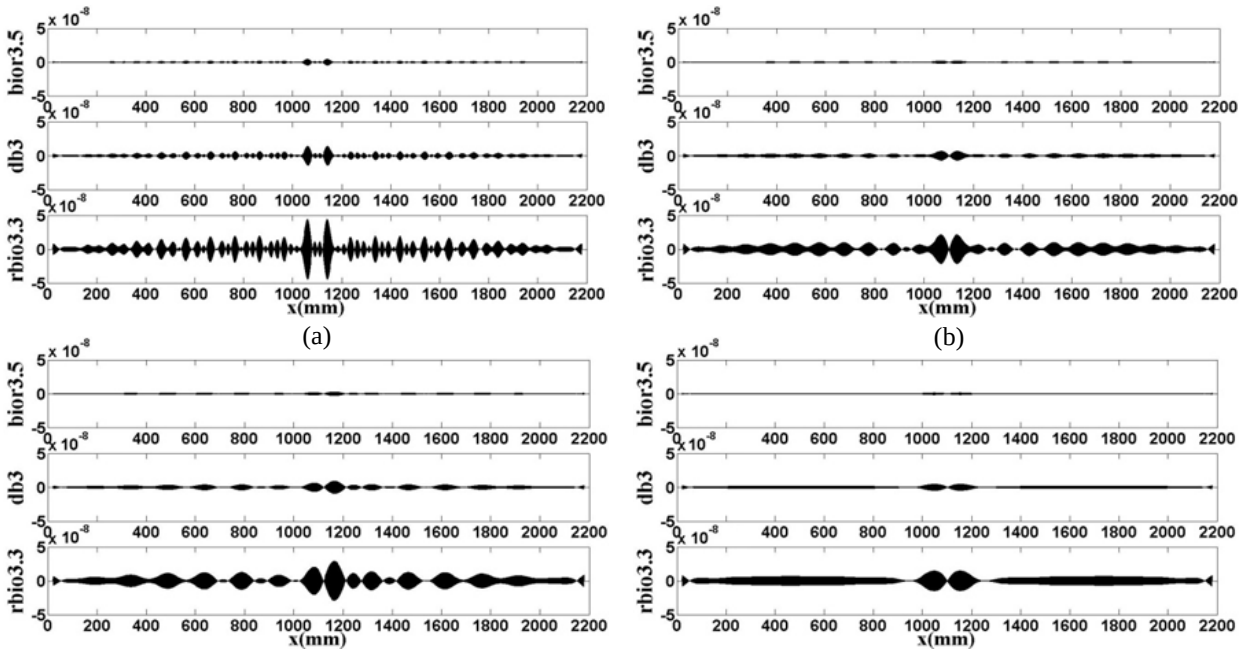

Fig. 13. Details signal of the first mode shape using bior3.5, db3 and rbio3.3 wavelets at sampling distance of: a) 25 mm; b) 50 mm; c) 75 mm and d) 100 mm.

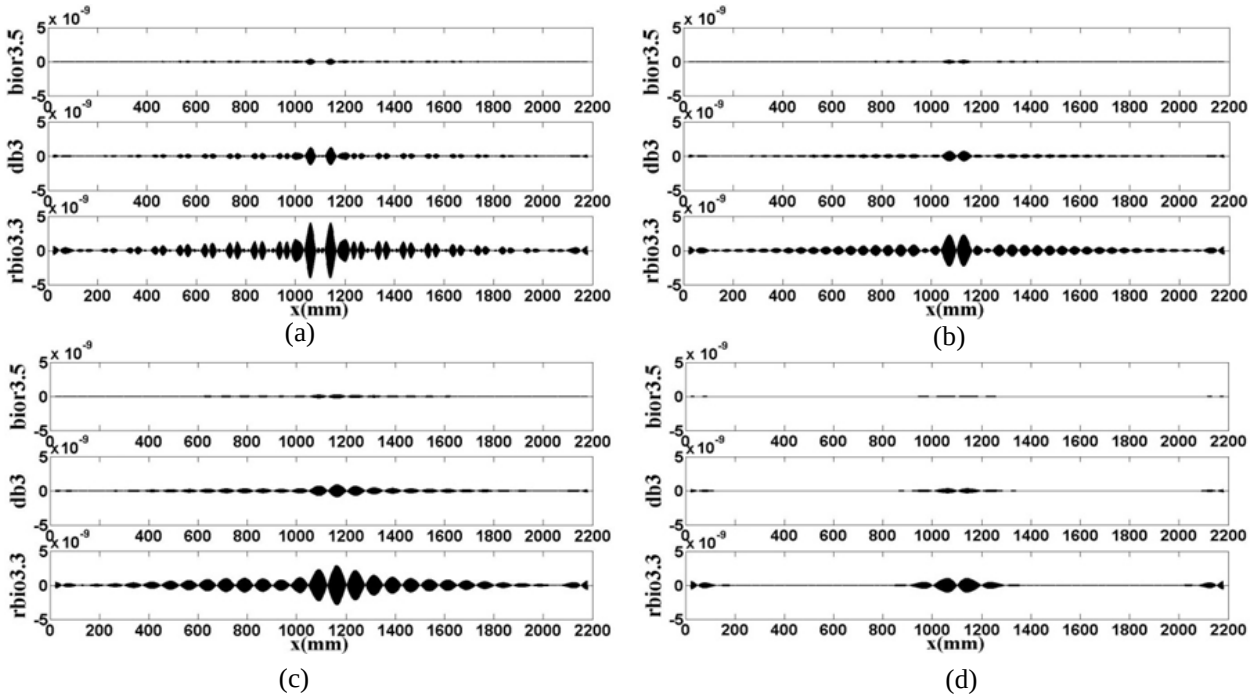

Fig. 14. Details signal of the first modal curvature using bior3.5, db3 and rbio3.3 wavelets at sampling distance of: a) 25 mm; b) 50 mm; c) 75 mm and d) 100 mm.

After choosing rbio2.2 and rbio3.3 as the replace for the similar wavelets, these two mother wavelets are compared to rbio2.4. Figs. 15 and 16 show the results of evaluation of these three cognate wavelets on the first mode shape and modal curvature, respectively.

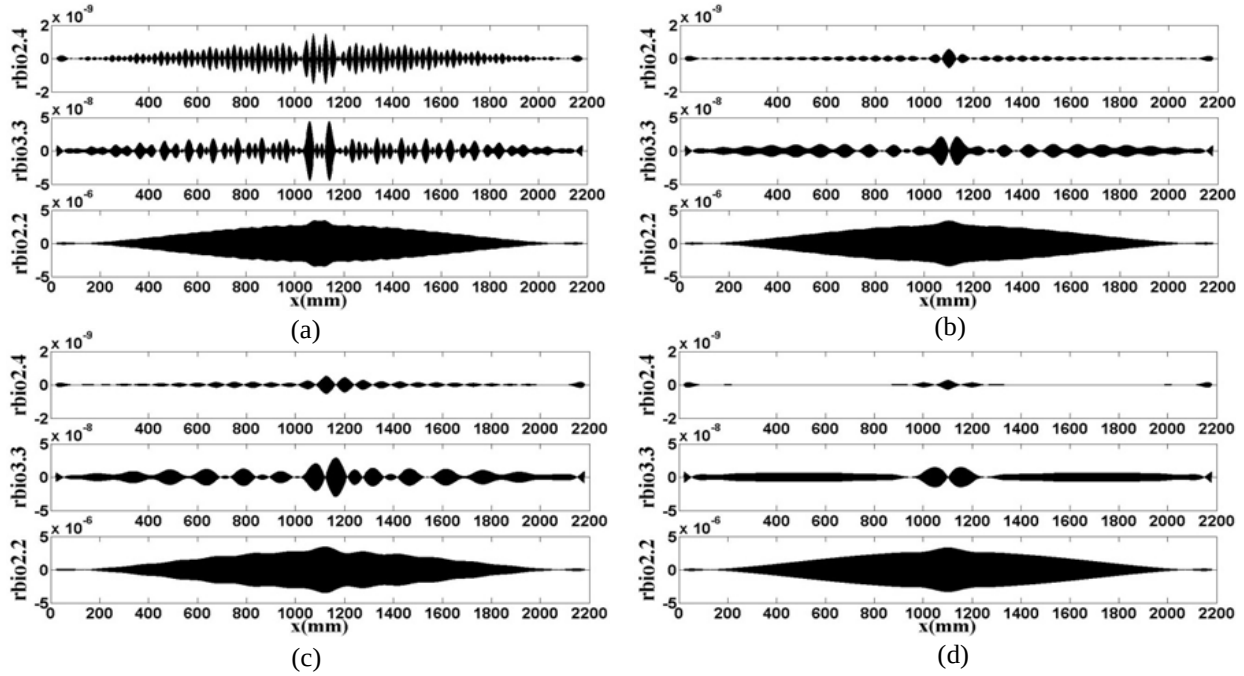

Fig. 15. Details signal of the first mode shape using rbio2.4, rbio3.3 and rbio2.2 wavelets at sampling distance of: a) 25 mm; b) 50 mm; c) 75 mm and d) 100 mm.

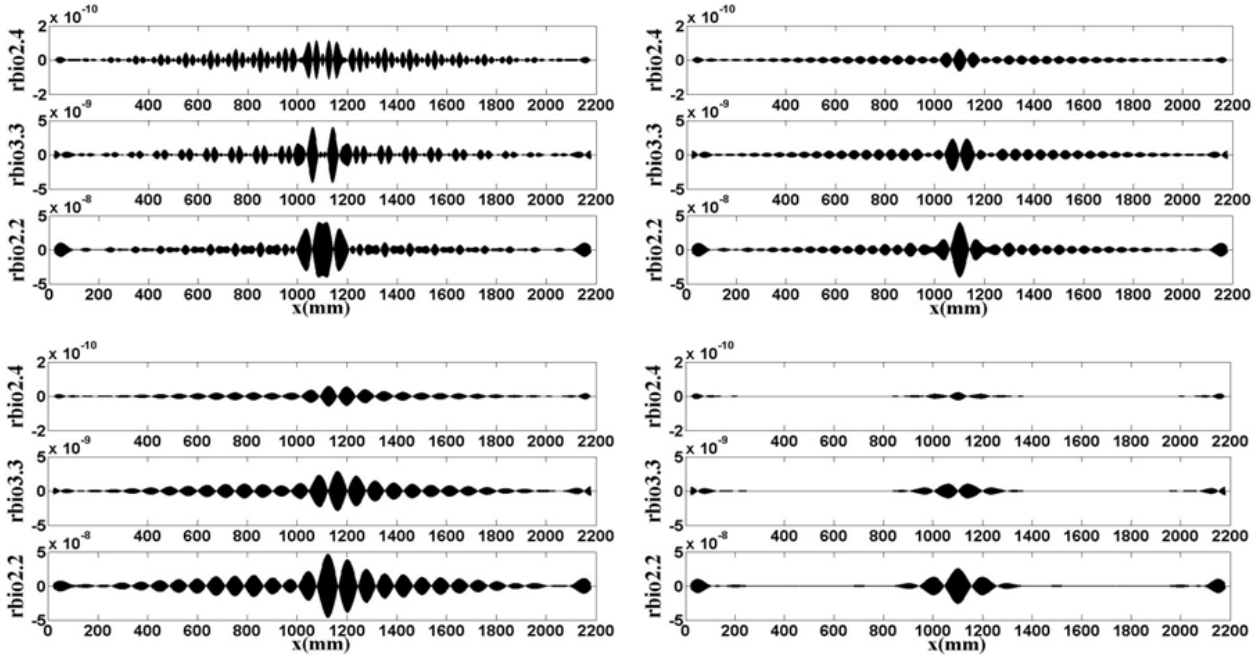

Fig. 16. Details signal of the first modal curvature using rbio2.4, rbio3.3 and rbio2.2 wavelets at sampling distance of: a) 25 mm; b) 50 mm; c) 75 mm and d) 100 mm.

As it could be found in Fig. 15, for the first mode shape, details signal calculated by using of rbio2.2 mother wavelet has a greater amplitude than rbio2.4 and rbio3.3; but the locating accuracy of this wavelet is low. Notwithstanding smaller range, rbio2.4 leads to a better result in damage locating compared to the two other. According to Fig. 16, for the first modal curvature, rbio2.2 has a greater amplitude and estimates location of damage better than the two others do.

Investigation of the details signals shows that, generally, modal strains are more sensitive to damage compared to vibration mode shapes. Moreover, in all cases, the signals calculated by use of mother wavelet rbio2.2 have greater amplitudes. Wavelets rbio2.4 and rbio2.2 give better results in locating damage for the first mode shape and for the first modal curvature, respectively. Regarding the degrees of freedom and sampling distances, as expected, increasing these distances leads to reduction of ability of the method for identification of accurate location of damage. Due to asymmetry of basic functions of some of the wavelets used in this section, the signals resulted from these wavelets in asymmetric sampling distance of 75 mm are unable to locate damages correctly.

4. Identifying damage locations

4.1. Proposed damage index

This section is focused on evaluation of application of the best mother wavelets on data obtained from numerical models. Since there are few vibration modes which measured practically, the first three mode shapes of the specimens were examined. Mode shapes were processed by central difference method and curve fitting by spline functions. The mode shapes and corresponding modal curvatures for numerical modes caused by the three damage scenarios are represented in Fig. 17. The degrees of freedom were considered with 100 mm distances from each other in order to be in agreement with experimental test.

According to Fig. 17, the affected mode shapes and corresponding modal curvatures by the damage scenario do not show considerable changes. In order to detect damage scenarios, as illustrated in in Fig. 18 and 19, respectively, the wavelet transform of mode shapes and corresponding modal curvatures were conducted by choosing rbio2.4 as the mother wavelet for mode shapes and rbio2.2 for modal curvatures. The vertical lines indicate damage locations.

As it can be seen in Fig. 18, as the same to many other damage detection methods, the proposed method has some problems in damage localization at the supports. For single damage scenario, the second mode is not able to detect damage location but the first and the third mode are able to detect it. The first and the second modes detect the location of double and triple artificial damages correctly but the third one is unable to do so. According to Fig. 19, similar to details signal of mode shapes, the wavelet coefficients obtained from modal curvatures do not have a correct estimation at supports. The second modal strain does not detect the location of single damage scenario correctly; also, the third modal curvature does not detect the location of double and triple artificial damage correctly.

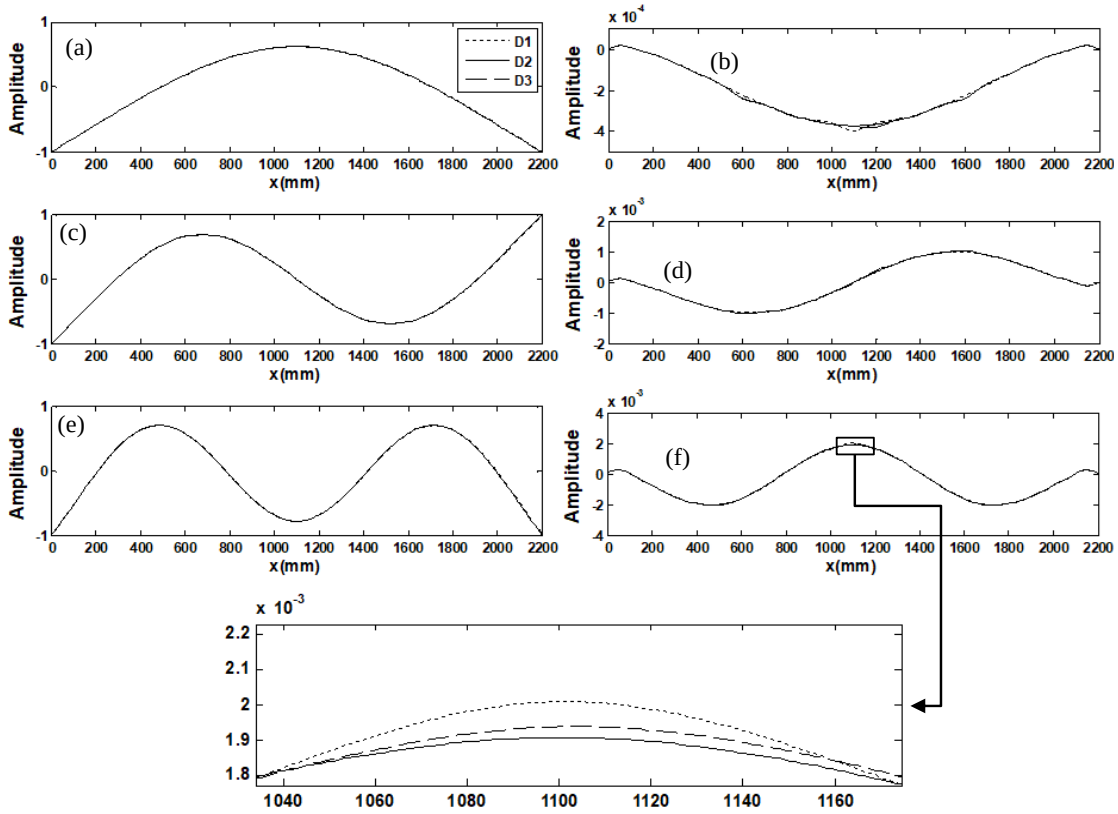

Fig. 17. First (a and b), second (c and d) and third (e and f) mode shapes and corresponding modal curvatures in the three damage scenarios.

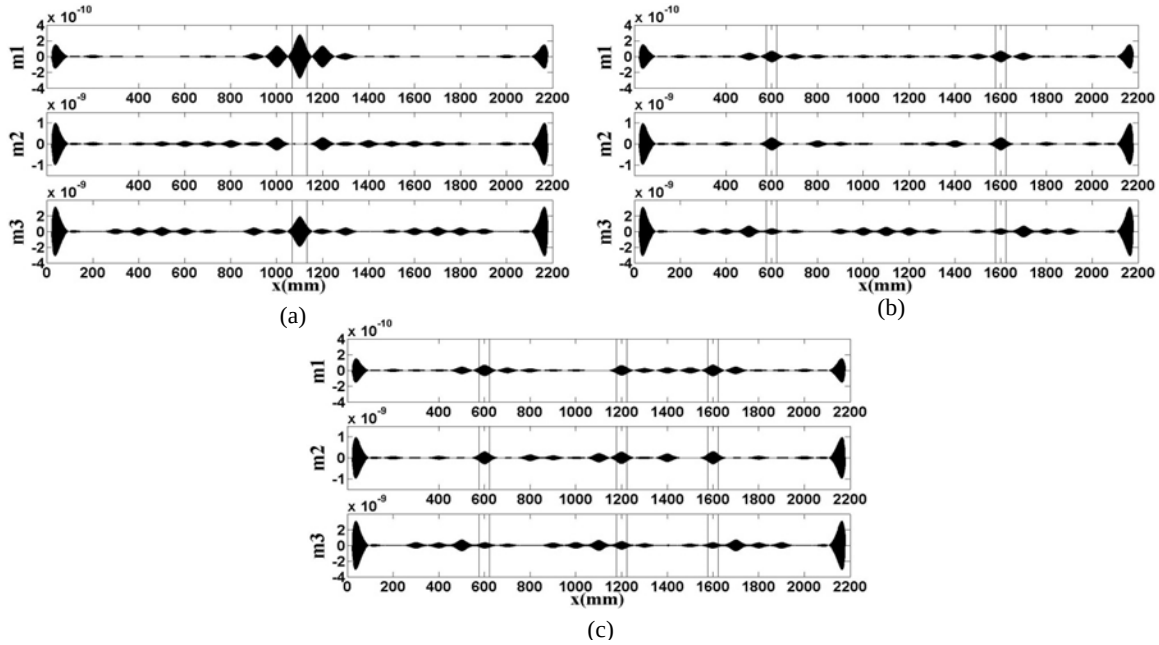

Fig. 18. Details signal of mode shapes using wavelet rbio2.4 for different damage scenarios: a) Single; b) Double and c) Triple.

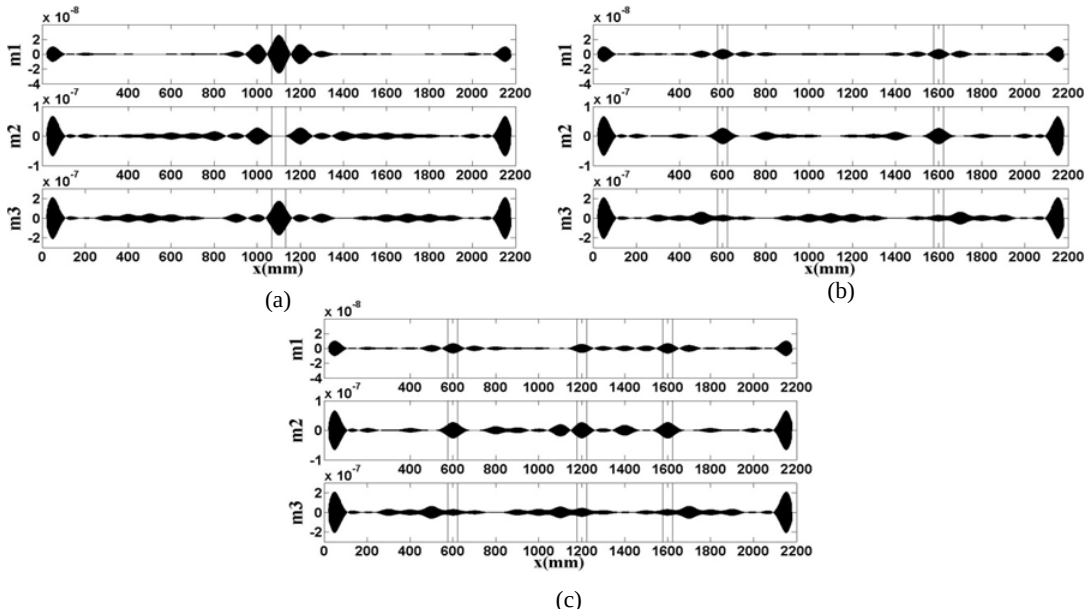

Fig. 19. Details signal of modal curvatures using wavelet rbio2.2 for different damage scenarios: a) Single; b) Double and c) Triple.

Comparing Figs. 18 and 19, it can be concluded that generally the details signal of modal curvature have greater amplitudes than mode shapes; which indicates their more sensitivity to damage. Moreover, the details signal obtained from mode shapes and their corresponding modal curvatures in different modes have different amplitudes. To specify location of damage scenarios better, and utilize the ability of all the modes, more processes is needed. Some researchers conduct these processes using statistical methods. One of these methods is hypothesis testing; which will be used in this paper. In hypothesis testing method the details signal (D_j) as a damage indicator is assumed a random variables which are normalized and resulted standard variables of z_j as follows [52]:

$$z_j = \frac{D_j - \mu_D}{\sigma_D} \tag{5}$$

Where z_j is the normalized damage index of jth component, μ_D is the mean and σ_D is standard deviation of D_js. Figs. 20 and 21 show the result of employing this index for mode shapes and their corresponding modal curvatures in three damage scenarios.

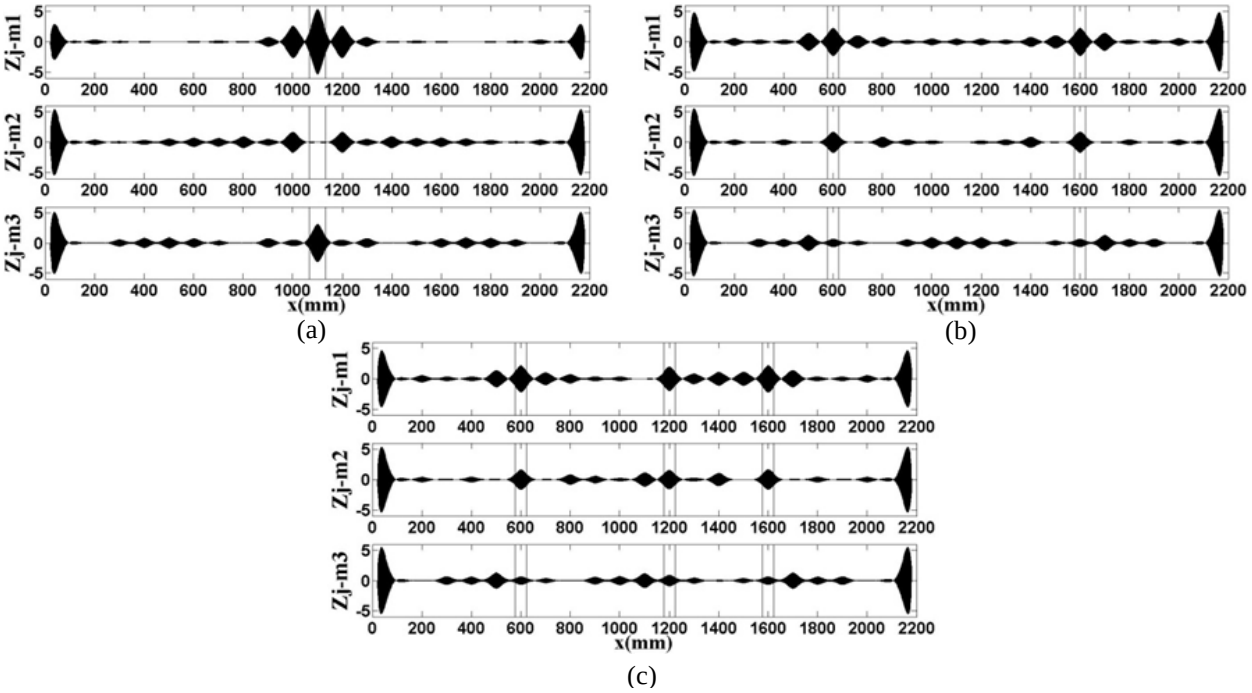

Fig. 20. Damage index (z_j) applied on mode shapes using rbio2.4 in different damage scenarios: a) Single; b) Double and c) Triple.

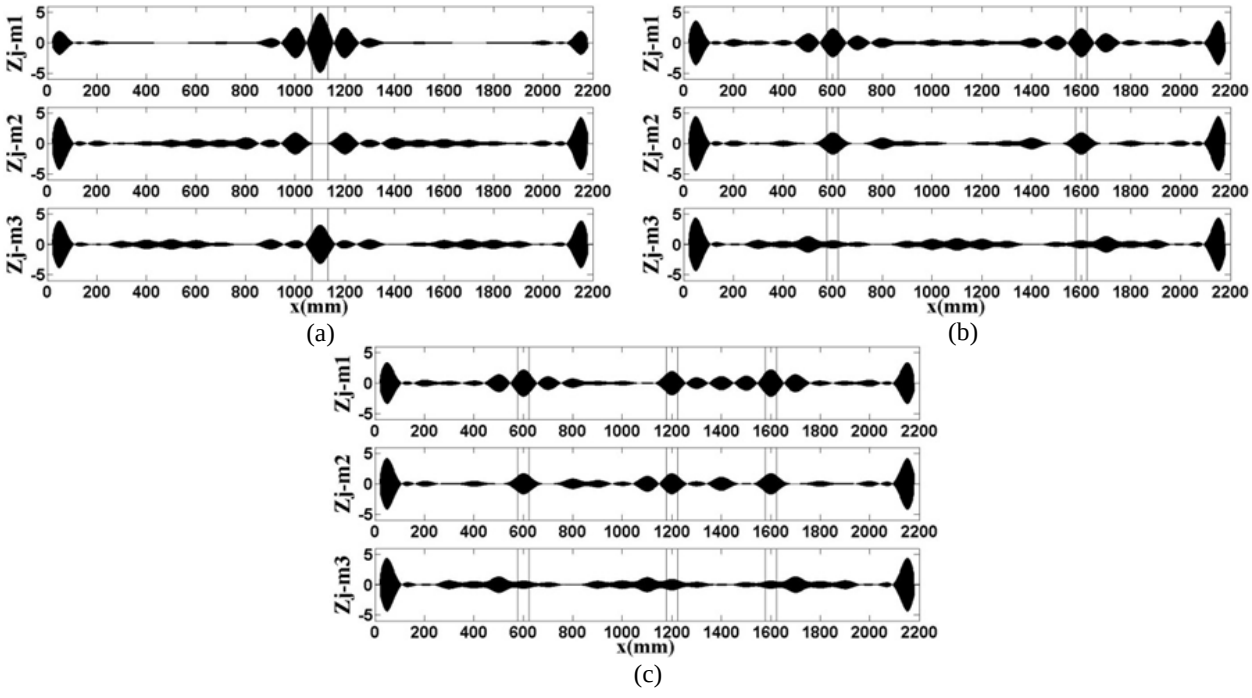

Fig. 21. Damage index (z_j) applied on modal curvatures using rbio2.2 in different damage scenarios: a) Single; b) Double and c) Triple.

As it can be seen in Figs. 20 and 21, the wavelet coefficients are normalized by using the z_j index; and it causes the decision making to be easier to determine sensitivity of different modes. For single damage scenario, all mode shapes and first and third modal curvatures could detect the location of damage successfully, and the first modal data are more sensitive. The second modal data are unable to detect single damage scenario. The first and the second modes, with almost the same sensitivity, have the ability to detect the locations of double and triple damage scenario but the third one is unable. The triple damage scenario could be detected by suing of the first and the second modes.

In order to represent damage location better, a threshold can be considered for damage indicator of z_j. This threshold is considered by assuming normal distribution of D_j variable and definition of z_n variable as the starting level of damage. If $z_j < z_\eta$, no damage is occurred, otherwise the component is damaged. With this definition, the values greater than the threshold remain that are considered as the estimated locations of damage and the smaller values are zeros. For this reason, the modified damage index (zr_j) has values greater than zero. Fig. 22 shows a schematic of applying threshold on normalized damage index (z_j).

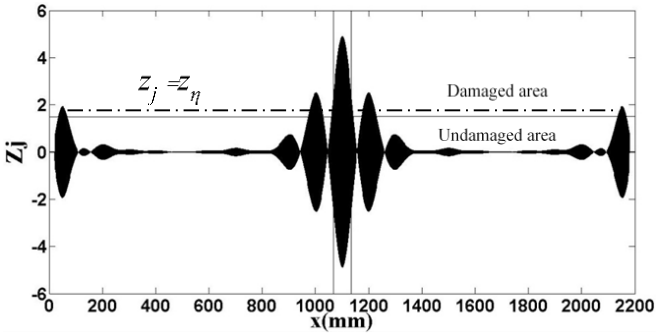

Fig. 22. The schematic of threshold application of zj normalized damage index.

In this paper, three damage scenarios were located by assuming threshold of z_η equal to 1.6. Figs. 23 and 24 demonstrate the result of the detection by using of modified damage indicator of zr_j for mode shapes and modal curvatures.

As we see in Figs. 23 and 24, modified damage index of zr_j shows the estimated damage locations are better after applying threshold; so it is more suitable for damage detection. By investigating modified damage index of zr_j, it can be concluded that in order to detect damage location in concrete beam specimens using the proposed method, a collection of various mode responses should be considered; and no decision can be made based on one specific mode. In addition, in order to address the problem of the method at support locations, application of windowing on the indicator will be useful. In this paper, with respect to the type of details signal, Turkey window is used for removing their bad results in support locations. As shown in Fig. 25, this window has a conical-cosine shape and is defined based on the length of the vector and the ratio of conical part to constant part as below [53]:

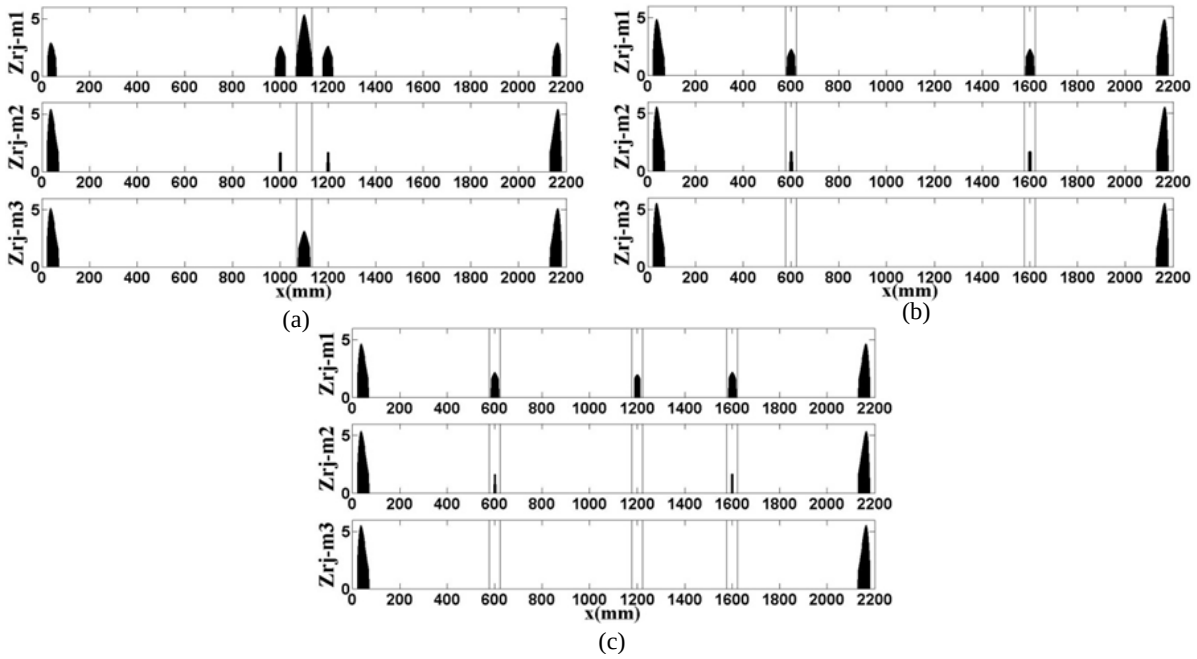

Fig. 23. Modified damage index of zr_j for mode shapes in different damage scenarios: a) Single; b) Double and c) Triple.

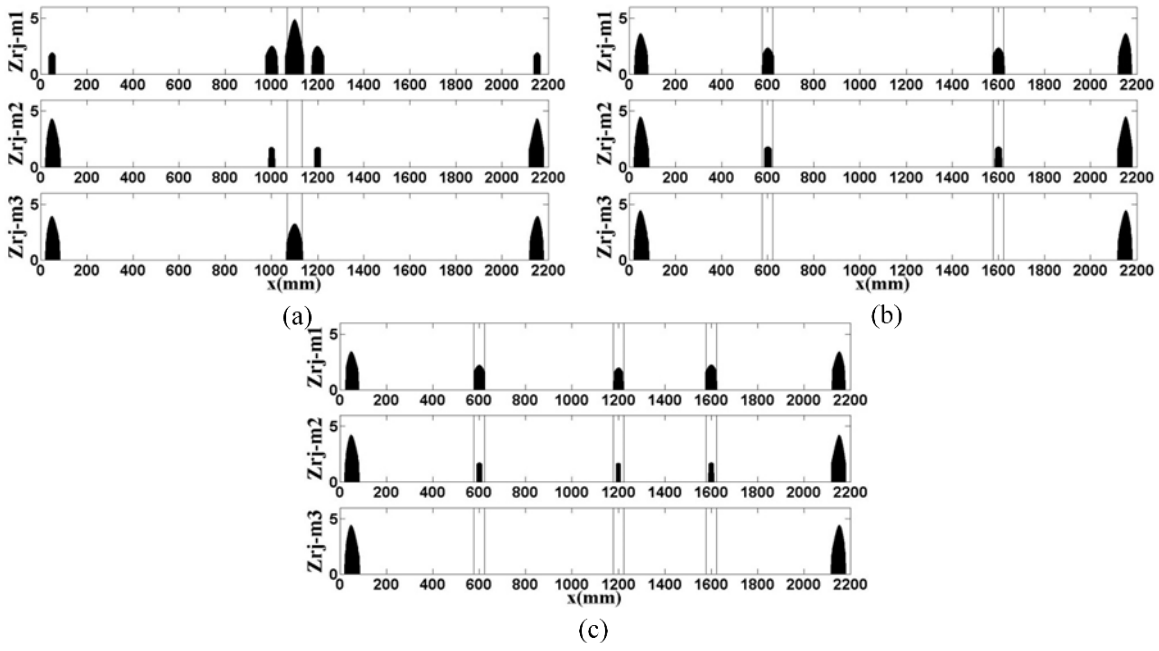

Fig. 24. Modified damage index of zr_j for modal curvature shapes in different damage scenarios: a) Single; b) Double and c) Triple.

$$w(x)=\begin{cases}\frac{1}{2}\{1+\cos(\frac{2\pi}{\alpha}[x-\alpha/2])\} & 0\le x\le\frac{\alpha}{2}\\ 1 & \frac{\alpha}{2}\le x<1-\frac{\alpha}{2}\\ \frac{1}{2}\{1+\cos(\frac{2\pi}{\alpha}[x-1+\alpha/2])\} & 1-\frac{\alpha}{2}\le x\le 1\end{cases} \quad (6)$$

Where x is the vector and α is the ratio of the conical part to the constant part; and its value varies 0 to 1 (i.e. $0 \le \alpha \le 1$). The form of this window is such that it can be coordinated with vector length by considering different αs. In this research, for removing the support effect in modified indicator of zr_j, biquadratic of the window with α=0.2 was applied. Fig. 26 shows this window.

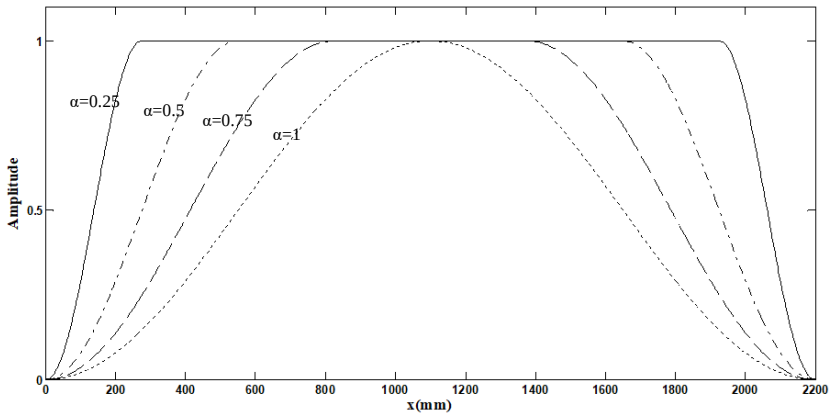

Fig. 25. Turkey window [53]

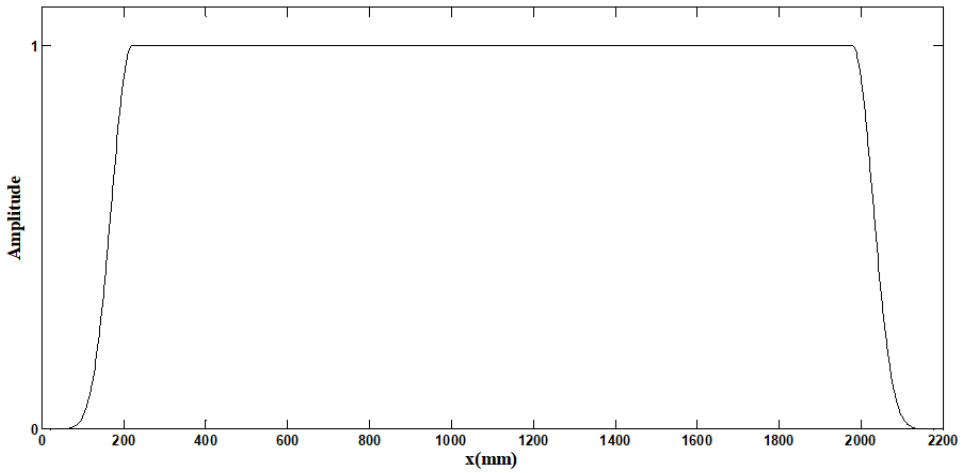

Fig. 26. The applied window

After applying the window on modified damage index of zr_j to find damaged locations in numerical model, the results of the index in different modes should be overlapped. Fig. 27 shows the outcome of overlapping, for each of damage scenarios in numerical model.

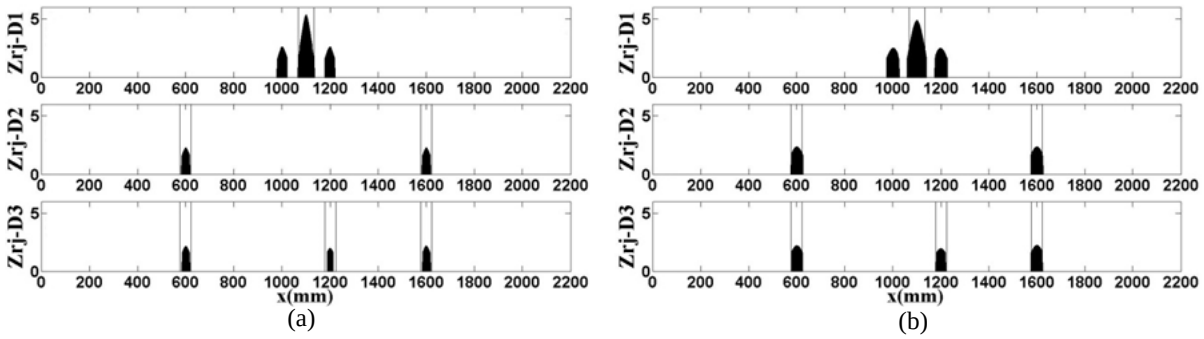

Fig. 27. Overlapping of modified index of zr_j in: a) mode shapes; b) modal curvatures

As it seen in Fig. 27, the suggested method detects the location of all damage scenarios for their corresponding mode shapes and modal strains correctly. So, overlapping of modified damage indicator of zr_j can be used after elimination of support effect for detection of damage locations in structures.

4.2. Noise contaminated modal data

In most experimental tests, there are many factors involved such as environmental conditions and noise. Sometimes, the effect of environmental conditions on modal data is more than damage effect and it led to a wrong decision. Noise affects the frequency response functions and changes them. The changes in these functions cause the mode shapes to be rough; so it causes data processing to be problematic. There are so many methods proposed for noise reduction up to now. Noise can be reduced in signals by modifying testing methods and applying a suitable isolator. Signal processing knowledge and modern data collecting devices help the researchers to be closer to this goal. But still, the remaining noise should be removd from collected data to calculate modal quantities. In this paper, as one of the signal processing methods, wavelet transforms are used for elimination of noise from modal data.

Donoho and Johnstone [54] showed that small coefficients existed in signals obtained from wavelet transform includes noise and have a little information of signal. Therefore, the noise-free version of signal can be achieved by ignoring these coefficients and by reconstruction of other coefficients of the wavelet. So, for noise elimination, firstly noisy data are considered as input signal for wavelet transform. Then, the details signal of the data is calculated by selected mother wavelet for denoising process. In the next stage, the smaller coefficients are eliminated by applying appropriate threshold; and the main signal is reconstructed by use of remaining wavelet coefficients. The resulted signal will be noise-free. Threshold application methods for noise isolation can be divided into two major category of hard and soft. In hard threshold application method the coefficients of the wavelet that their absolute values are less than a specific value are considered zero and the remaining coefficients remains with no change. How the hard threshold is applied is shown in Eq. (7) [54].

$$y = \begin{cases} x & |x| \geq \sigma \\ 0 & |x| \leq \sigma \end{cases} \tag{7}$$

Where σ is a specific value for threshold and x represents small coefficient. Method of soft threshold application is the developed form of hard method. In this method, the coefficients that are smaller than threshold are considered zero and then the remaining coefficients will be concentrated and shrank toward zero. The method is expressed as Eq. (8) [54].

$$y = \begin{cases} sign(x).(|x| - \sigma) & |x| \geq \sigma \\ 0 & |x| \leq \sigma \end{cases} \tag{8}$$

The method of soft threshold application is based on the fact that any wavelet coefficient includes a part of main signal and noise; and by application of this method, noises will be isolated from coefficients and the main signal will remain. Donoho [55] defined his general law for threshold as below:

$$\sigma = s\sqrt{2\log(n)} \tag{9}$$

Where n is signal length and s is standard deviation of the estimated noise. Noise can be eliminated from the signal by considering the threshold and using one of the isolation methods; then the noise-free signal can be used for the next processes [55].

In this paper, in order to evaluate the ability of the wavelets for damage detection using noisy data, two types of noise called High-frequency Noise and White Gaussian Noise were added in the form of vibration modes resulted from B1 specimen in three damage scenarios. The following equation was used for simulation of the noise type I (High-frequency Noise):

$$Data_{Noise} = Data_{Noise-free} + 0.01\sin(95\pi t) \tag{10}$$

According to this equation, frequency of the noise has been considered 95 *Hz*. The three first mode shapes with this noise are shown in Fig. 28.

The effect of noise is recognizable in all the mode shapes showed in Fig. 28. It shows that for a small damage, the irregularities that have been developed in data due to damage may be confused with the irregularities caused by noise effect. Also for the relatively large damages, these irregularities may cause problem in detection of the correct location of damage.

In this paper, the soft isolation method is used for reduction of the effect of these noises. The threshold for noise isolation has been considered σ = 0.00745; and in order to apply the soft method, the symmetric wavelet with 8 vanishing moments (sym8) has been used. Fig. 29 shows the outcome of noise elimination from the three vibration mode shapes.

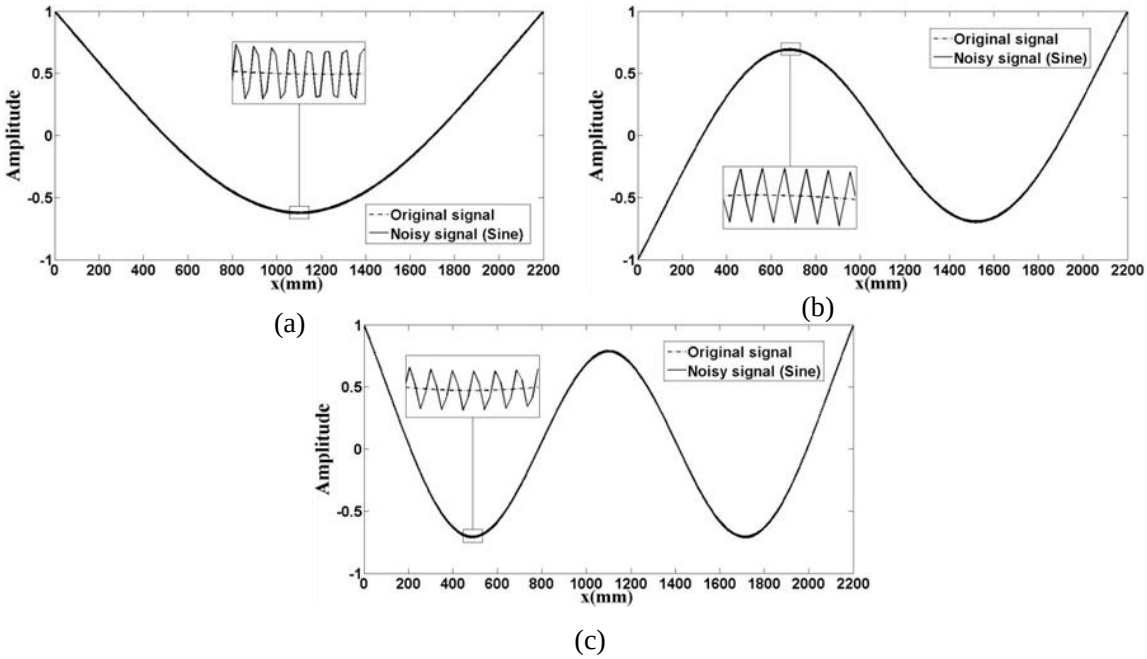

Fig. 28. The mode shapes contaminated by the noise type I: a) first mode; b) second mode and c) third mode.

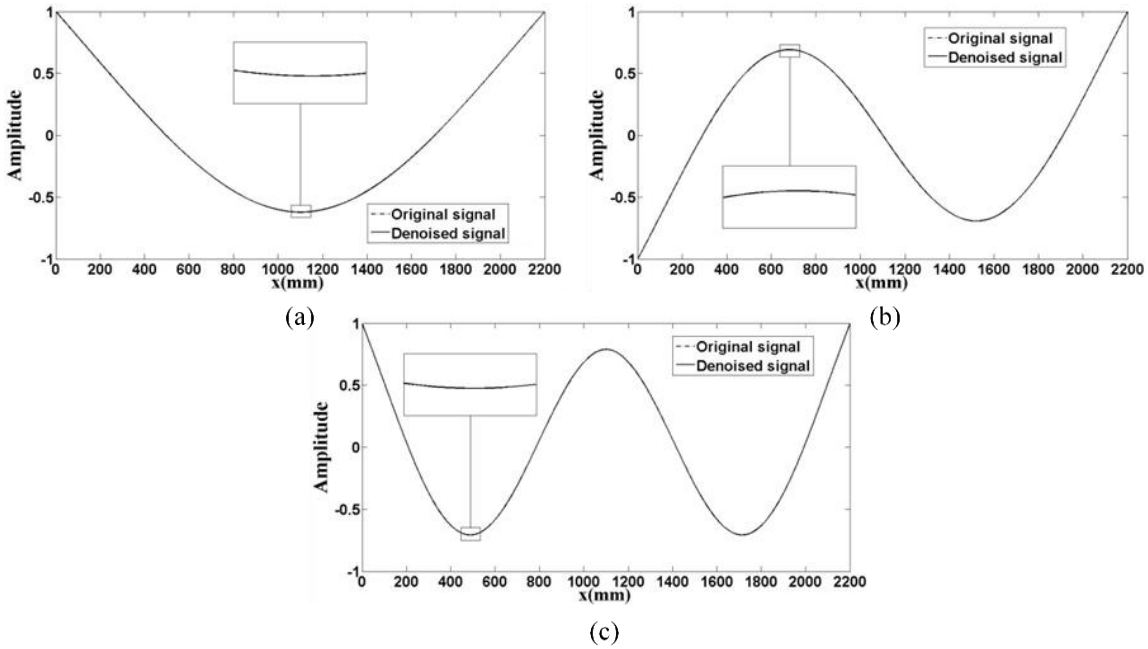

Fig. 29. The primary noise-free mode shapes for noise type I: a) first mode; b) second mode and c) third mode.

As seen in Fig. 29, after presentation of the mode shapes having noise type I by soft isolation method, the effect of noises is reduced fairly.

For simulation of noise type II, random number generator of MATLAB was used to develop White Gaussian Noise. The random numbers were between 0 and 1. The noise is obtained by Eq. (11) as following:

$$Data_{Noise} = (1 + e \times (2 \times rand - 1)) \times Data_{Noise-free} \tag{11}$$

In this equation, e represents the amount of noise. As shown in Fig. 30, the mode shapes having this type of noise are demonstrated. Fig. 32 shows that the noise type II has an unpredictable irregular behavior; also it is more similar to the data occurred in real world compared to noise type I. The outcome of soft isolation of this noise from vibration mode shapes is shown in Fig. 31.

As seen in Fig. 31, isolation of noise from mode shapes having noise type II eliminated the effect of this noise as much as possible but it was less successful than noise type I. After isolation of noise from data, the ability of modified damage index zr_j in detection of damage in noisy data is evaluated. For this end, details signals were obtained for three damage scenarios by presenting noise-removed mode shapes to rbio2.4 wavelet transform. Then, the damage scenarios were detected by using of hypothesis testing method and applying threshold of z_n = 1.15 for noise type I and z_n = 1.6 for noise type II. Figs. 32 and 33 show the results of zr_j index for type I and type II noises, respectively.

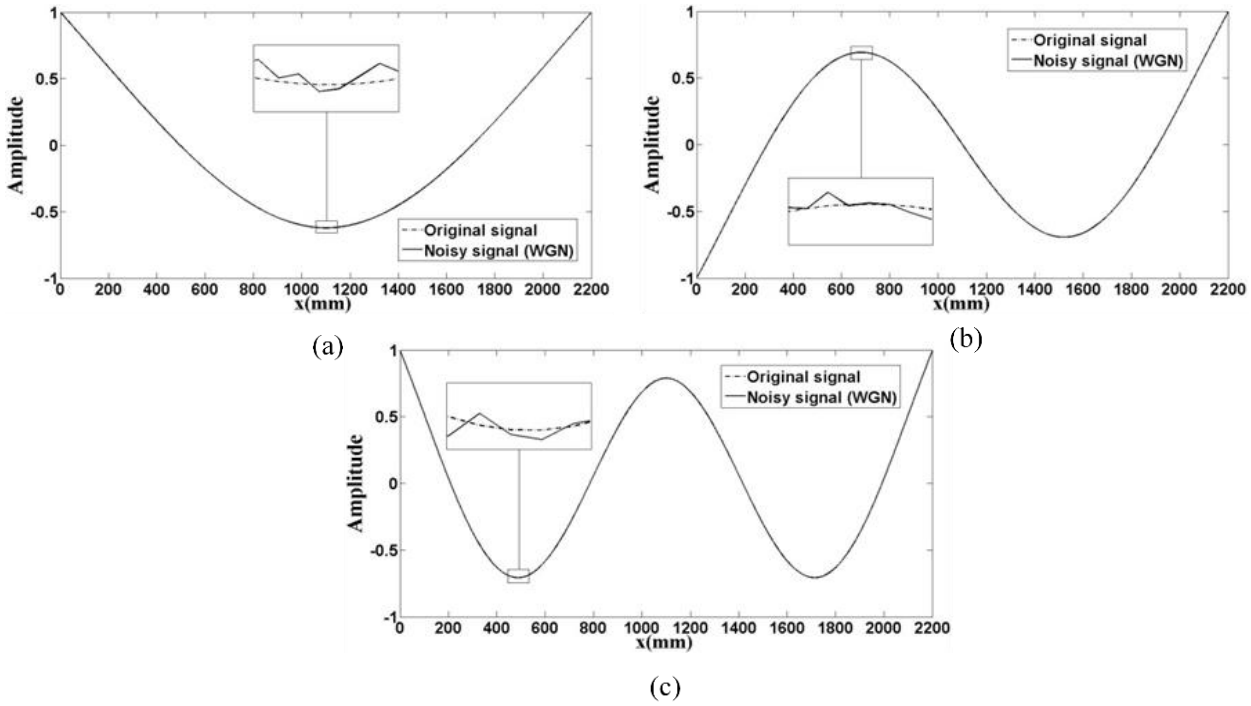

Fig. 30. The mode shapes contaminated by noise type II: a) first mode; b) second mode and c) third mode.

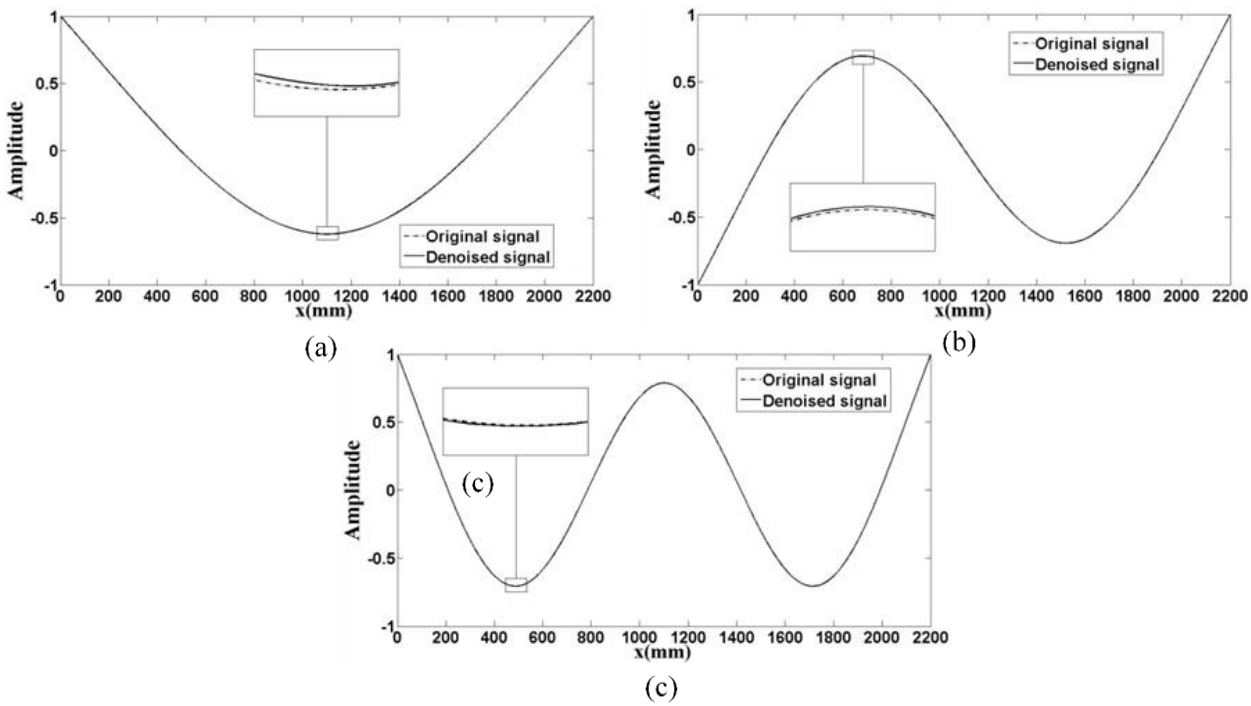

Fig. 31. The primary noise-free mode shapes for noise type II: a) first mode; b) second mode and c) third mode.

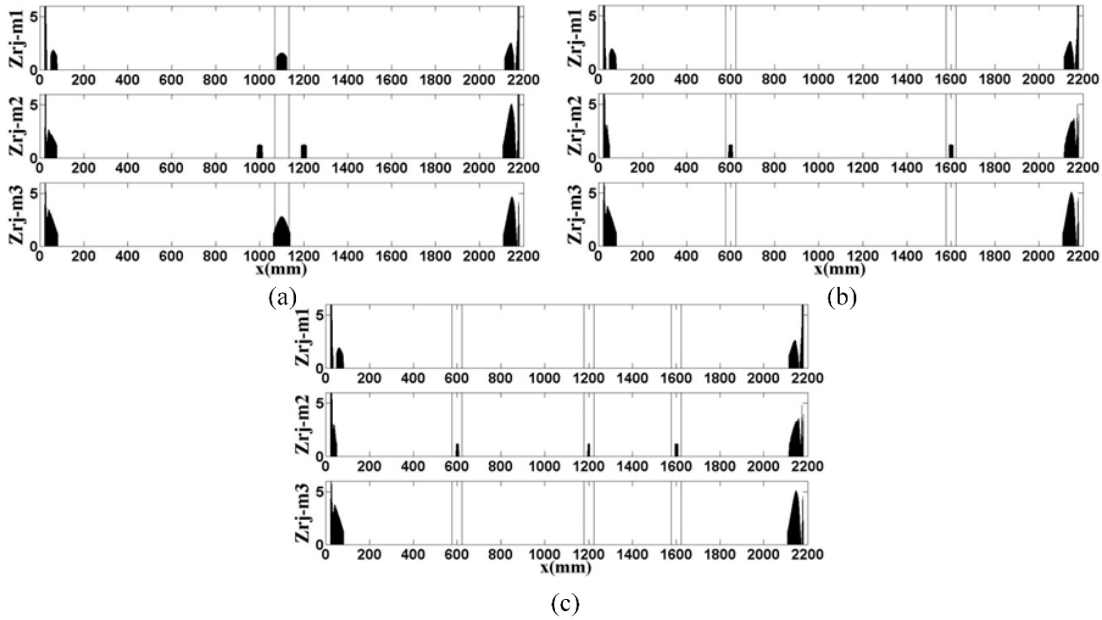

Fig. 32. zr_j index for vibration mode shapes having noise type I in different damage scenarios: a) single; b) double and c) triple.

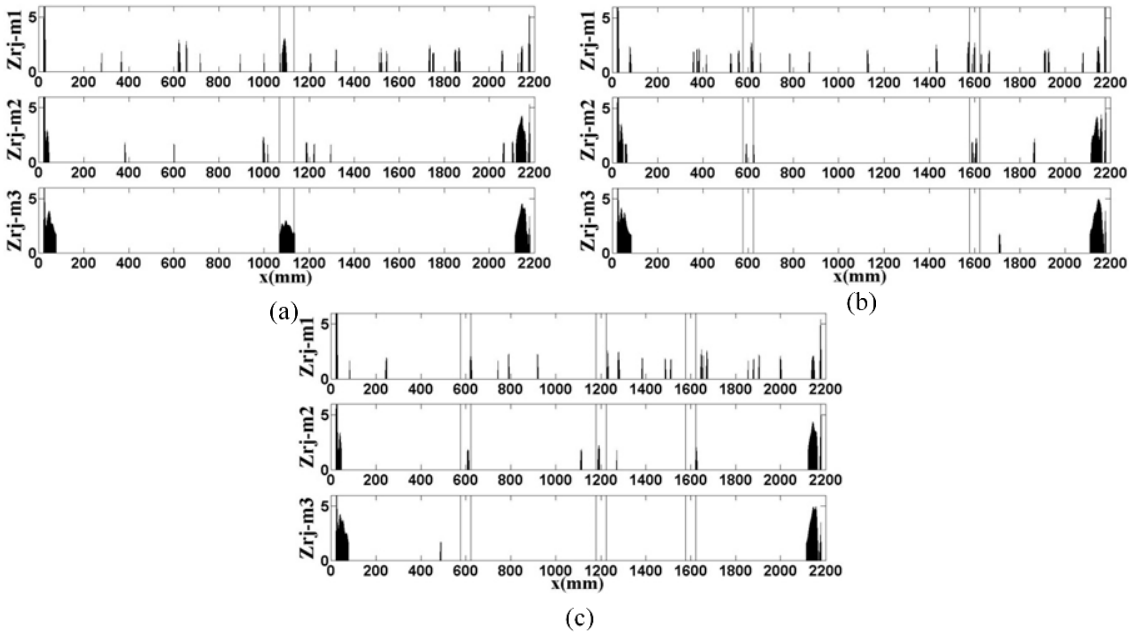

Fig. 33. zr_j indicator for vibration mode shapes having noise type II in different damage scenarios: a) single; b) double and c) triple.

According to Fig. 32, notwithstanding initial noise in mode shapes, zr_j damage index was successful in detection of damage locations. The location of single damage scenario was correctly detected by the first and third mode shapes; also the location of double and triple damage scenarios were correctly detected by the first and third mode shapes. The results of Fig. 33, the denoising method is not successful on the mode shapes having noise type II and it is unable to detect the correct location of damage in any of damage scenarios. The nature of both artificial Type I and Type II noises were randomly added high frequency low domain signals, which in most real field and also experimental condition, most of previously proposed damage detection methods are unable to clarify and make distinction between if the presented fluctuation in input signal are related to real damage condition or it is just originated from the environmental noises. Therefore, determining the type of fluctuations and singularities in input signals (if it is originated from environmental noise or real damage condition) is the most challenging issue in current damage detection investigations. Therefore, in this paper, to overcome this regular challenge, instead of using the mode shapes, modal curvatures were utilized as input signals. The details signal of modal strain of the specimens were examined in order to improve the proposed method and for comparing ability of noise isolation method in vibration mode shapes and their modal strains as well. After isolation of noise from mode shapes, their modal curvatures were obtained by central difference method. Details signal of strains was calculated by using of rbio2.2 wavelet and z_j coordinated indicator was achieved. Then, the damages were assessed by applying a threshold of z_n = 1.3 for noise type I and z_n = 1.24 for noise type II. Fig. 34 and 35 show the results of assessment for modal curvatures having these two types of noise.

According to Fig. 34 for noise type I, modal curvatures could detect locations of damage scenarios as well as mode shapes. Therefore, it can be concluded that for regular high frequency noises the isolation method can have a good performance for both vibration modes and modal

curvatures. Fig. 35 shows that unlike the result of applying the proposed method on shape modes having noise type II, which was not able to damage scenarios localization, applying this method on modal curvatures can lead to a suitable estimation of damage scenarios locations. Hence, as expected, modal curvatures are more sensitive to damages compared to vibration mode shapes; and the can be used for damage detection in practice.

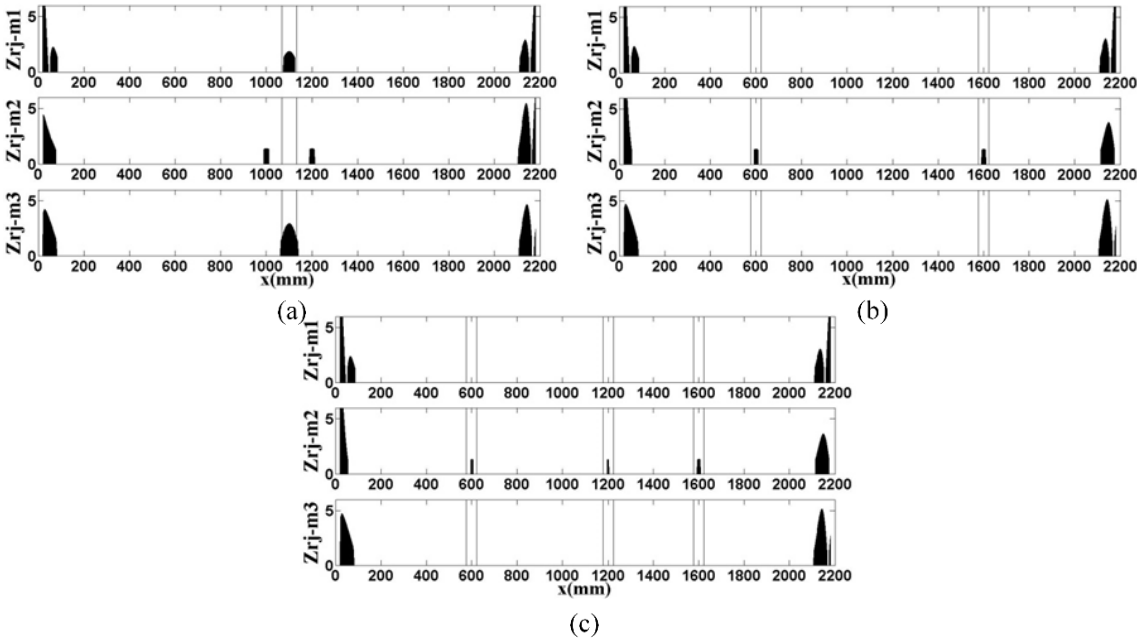

Fig. 34. zr_j index for modal curvatures having noise type I in different damage scenarios: a) single; b) double and c) triple.

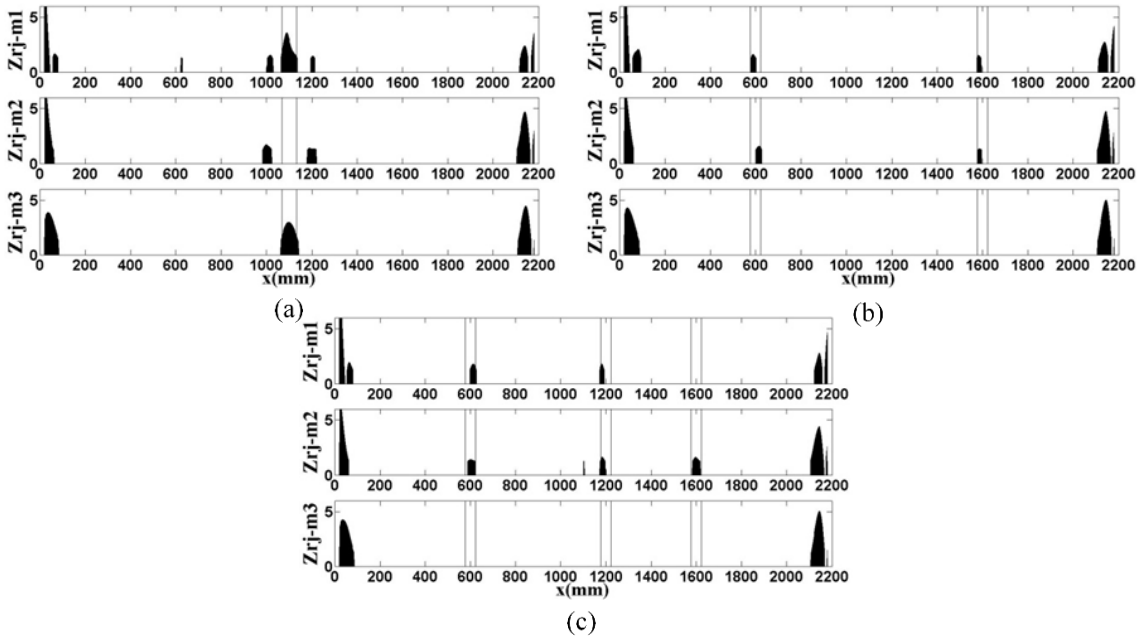

Fig. 35. zr_j index for modal curvatures having noise type II in different damage scenarios: a) single; b) double and c) triple.

A notable point in Fig. 34 and 35 is extreme sensitivity of the method to supports and wrong estimation of damage location at support points. Also, just a few mode shapes and modal curvatures are able to detect damages. In order to reach a single method, overlapping of different mode responses as well as windowing will be used for elimination of support effects. Figs. 36 and 37 show the results of this equalization for mode shapes and modal curvatures contaminated with both noise types.

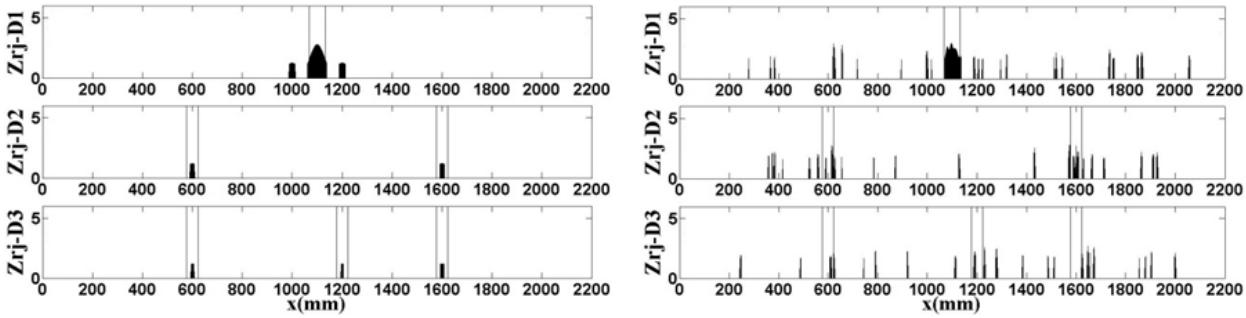

Fig. 36. Accumulation of zr_j index for mode shapes contaminated with: a) noise type I and b) noise type II

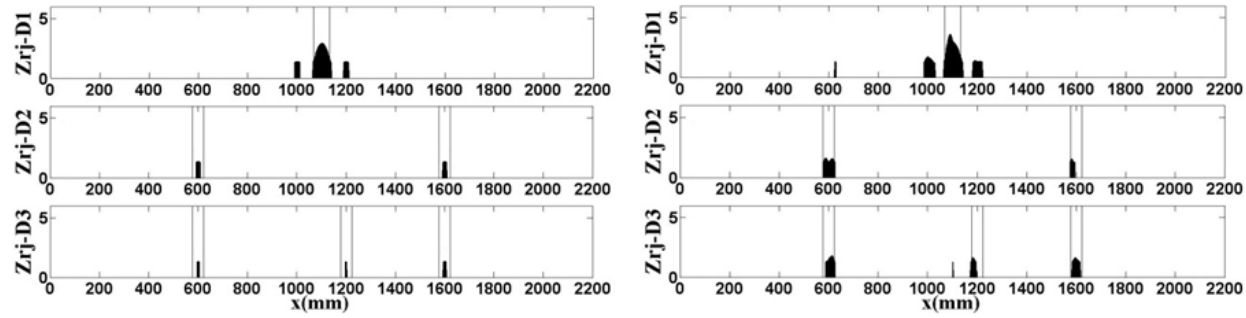

Fig. 37. Accumulation of zr_j index for modal curvatures contaminated with: a) noise type I and b) noise type II.

Analyzing Figs. 36 and 37 shows that for noise type I, the damage index obtained from vibration mode shapes and modal curvatures have detected damage location correctly. This success for noise type II is only seen in damage index calculated by modal curvatures. Noises of experimental modal data are irregular and are more similar to noise type II. Therefore, the vibration mode shapes cannot be used for damage detection using real modal data in practice; and it is necessary to calculate modal curvatures.

5. Conclusions

The goal of this paper is to propose a wavelet based damage index to identify damage locations in RC beams. To achieve this goal, single, double and triple damage scenarios were applied in numerical models of RC beams which were simulated based on an experimental specimen.

Considering mode shape and modal curvatures as input signals of Wavelet transform, a damage index is proposed based on the resulted Wavelet coefficients. Different Wavelets mothers including bior2.4 and bior3.5 from Biorthogonal wavelet family, db2 and db3 from Daubechies family and rbio2.2, rbio2.4 and rbio3.3 from Reverse Biorthogonal family were compared to select the most proper one. In addition, the influence of various sampling distances of 25 mm, 50 mm, 75 mm and 100 mm on damage localization accuracy were investigated. In addition, in order to simulate the practical conditions, two kind of noises were added to modal data and deniosed by wavelet denoising techniques, before introducing them as inputs to damage index. It should be mentioned that the boundary effect and detecting damage locations near the boundaries is the only limitation of the proposed damage detection method. To overcome this limitation, as presented in modal tests details, the structural element would be hanged on in a suspended condition to eliminate the effects of boundaries on obtained modal data. The following results were obtained in this study:

- Investigation of different wavelets for localization of damage scenarios revealed that rbio2.4 and rbio2.2 have better performance for wavelet analyzing of mode shapes and modal curvatures, respectively. Moreover, the detail signals using rbio2.2 mother wavelet has a greater amplitude and shows more sensitivity to presence of damages.
- Evaluation of details signals show that generally modal curvatures are more sensitive to damage scenarios in comparison with mode shapes.
- As expected, increasing sampling distances causes a performance reduction in proposed method in detection of accurate location of damage scenarios. In addition, due to symmetry of basic functions of some of the wavelets used in this paper, the detail signals obtained from these wavelets failed to detect damage location correctly in asymmetric sampling distance of 75 mm.
- The results of application of the damage index obtained from hypothesis testing showed that it cannot be decided based on one specific mode for detection of damage location in concrete beam specimen. Moreover, the proposed method has a poor estimation of damages at support places. For this reason, Turkey window and overlapping of results were applied and the locations of damages were correctly revealed by introducing modified damage index.
- Examining the noise contaminated modal data showed that the damage index obtained from mode shapes and modal strains for noise type I was able to detect damage location accurately. This success for noise type II is only seen in damage index calculated by modal curvatures. Because of more similarity of real data to noise type II, modal curvatures and wavelet rbio2.2 were proposed as the best input signals and most proper mother wavelet.

Funding

This research received no external funding.

Conflicts of interest

The authors declare no conflict of interest.

References

[1] Karimipour A, Edalati M. Shear and flexural performance of low, normal and high-strength concrete beams reinforced with longitudinal SMA, GFRP and steel rebars. Eng Struct 2020;221:111086. https://doi.org/10.1016/j.engstruct.2020.111086.

[2] Karimipour A, Ghalehnovi M. Comparison of the effect of the steel and polypropylene fibres on the flexural behaviour of recycled aggregate concrete beams. Structures 2021;29:129–46. https://doi.org/10.1016/j.istruc.2020.11.013.

[3] Ghalehnovi M, Karimipour A, Anvari A, de Brito J. Flexural strength enhancement of recycled aggregate concrete beams with steel fibre-reinforced concrete jacket. Eng Struct 2021;240:112325. https://doi.org/10.1016/j.engstruct.2021.112325.

[4] Chaboki HR, Ghalehnovi M, Karimipour A, de Brito J, Khatibinia M. Shear behaviour of concrete beams with recycled aggregate and steel fibres. Constr Build Mater 2019;204:809–27. https://doi.org/10.1016/j.conbuildmat.2019.01.130.

[5] Jahangir H, Esfahani MR. Damage localization of Structures Using Adaptive Neuro-Fuzzy Inference System. 7th Natl. Congr. Civ. Eng., Zahedan, Iran: 2013.

[6] Daneshvar MH, Gharighoran A, Zareei SA, Karamodin A. Early damage detection under massive data via innovative hybrid methods: application to a large-scale cable-stayed bridge. Struct Infrastruct Eng 2020:1–19. https://doi.org/10.1080/15732479.2020.1777572.

[7] Jahangir H, Esfahani MR. Numerical Study of Bond – Slip Mechanism in Advanced Externally Bonded Strengthening Composites. KSCE J Civ Eng 2018;22:4509–18. https://doi.org/10.1007/s12205-018-1662-6.

[8] Jahangir H, Esfahani MR. Investigating loading rate and fibre densities influence on SRG - concrete bond behaviour. Steel Compos Struct 2020;34:877–89. https://doi.org/10.12989/scs.2020.34.6.877.

[9] Jahangir H, Esfahani MR. Experimental analysis on tensile strengthening properties of steel and glass fiber reinforced inorganic matrix composites. Sci Iran 2020. https://doi.org/10.24200/SCI.2020.54787.3921.

[10] Bagheri M, Chahkandi A, Jahangir H. Seismic Reliability Analysis of RC Frames Rehabilitated by Glass Fiber-Reinforced Polymers. Int J Civ Eng 2019. https://doi.org/10.1007/s40999-019-00438-x.

[11] Hasani H, Jahangir H, Rezazadeh Eidgahee D, Nasseri HR. Behavior Investigation of Rectangular Concrete Columns Confined by Fiber Reinforced Polymer Composites. 2nd Conf. Urban Planning, Archit. Civ. Eng. Environ., Oslo, Norway: 2021.

[12] Taherian I, Ghalehnovi M, Jahangir H. Analytical Study on Composite Steel Plate Walls Using a Modified Strip Model. 7th Int. Conf. Seismol. Earthq. Eng., 2015.

[13] Santandrea M, Imohamed IAO, Jahangir H, Carloni C, Mazzotti C, De Miranda S, et al. An investigation of the debonding mechanism in steel FRP- and FRCM-concrete joints. 4th Work. New Boundaries Struct. Concr., Capri Island, Italy: 2016, p. 289–98.

[14] Jahangir H, Bagheri M. Evaluation of Seismic Response of Concrete Structures Reinforced by Shape Memory Alloys (Technical Note). Int J Eng 2020;33. https://doi.org/10.5829/ije.2020.33.03c.05.

[15] Hasani H, Jahangir H, Rezazadeh Eidgahee D, Nasseri HR. Evaluation of Existing Axial Compressive Strength Models of FRP-Confined Circular Concrete Columns. 4th Int. Conf. 5th Natl. Conf. Civ. Eng. Archit. Art Urban Des., Tabriz, Iran: 2021.

[16] Jahangir H, Daneshvar Khoram MH, Esfahani MR. Application of vibration modal data in gradually detecting structural damage (In Persian). 4th Int. Conf. Acoust. Vib., Tehran, Iran: 2014.

[17] Altunışık AC, Okur FY, Karaca S, Kahya V. Vibration-based damage detection in beam structures with multiple cracks: modal curvature vs. modal flexibility methods. Nondestruct Test Eval 2019;34:33–53. https://doi.org/10.1080/10589759.2018.1518445.

[18] Daneshvar MH, Gharighoran A, Zareei SA, Karamodin A. Damage Detection of Bridge by Rayleigh-Ritz Method. J Rehabil Civ Eng 2020;8:111–20. https://doi.org/10.22075/JRCE.2019.17603.1337.

[19] Jahangir H, Esfahani MR. Structural Damage Identification Based on Modal Data and Wavelet Analysis. 3rd Natl. Conf. Earthq. Struct., Kerman, Iran: 2012.

[20] Seyedi SR, Keyhani A, Jahangir H. An Energy-Based Damage Detection Algorithm Based on Modal Data. 7th Int. Conf. Seismol. Earthq. Eng., International Institute of Earthquake Engineering and Seismology (IIEES); 2015, p. 335–6.

[21] Pahlevan Mosavari, A. Jahangir H, Esfahani MR. The Effect of Sensor Weight on Obtained Data from Modal Tests (In Persian). 9th Natl. Congr. Civ. Eng., Mashhad, Iran: Ferdowsi University of Mashhad; 2016.

[22] Naderpour H, Fakharian P. A synthesis of peak picking method and wavelet packet transform for structural modal identification. KSCE J Civ Eng 2016;20:2859–67. https://doi.org/10.1007/s12205-016-0523-4.

[23] Salawu OS. Detection of structural damage through changes in frequency: a review. Eng Struct 1997;19:718–23. https://doi.org/10.1016/S0141-0296(96)00149-6.

[24] Pandey AK, Biswas M, Samman MM. Damage detection from changes in curvature mode shapes. J Sound Vib 1991;145:321–32. https://doi.org/10.1016/0022-460X(91)90595-B.

[25] Dawari VB, Vesmawala GR. Modal Curvature and Modal Flexibility Methods for Honeycomb Damage Identification in Reinforced Concrete Beams. Procedia Eng 2013;51:119–24. https://doi.org/10.1016/j.proeng.2013.01.018.

[26] Wei Fan, Pizhong Qiao. Vibration-based Damage Identification Methods: A Review and Comparative Study. Struct Heal Monit 2011;10:83–111. https://doi.org/10.1177/1475921710365419.

[27] Ciambella J, Vestroni F. The use of modal curvatures for damage localization in beam-type structures. J Sound Vib 2015;340:126–37. https://doi.org/10.1016/j.jsv.2014.11.037.

[28] Hu H, Wang B-T, Lee C-H, Su J-S. Damage detection of surface cracks in composite laminates using modal analysis and strain energy method. Compos Struct 2006;74:399–405. https://doi.org/10.1016/j.compstruct.2005.04.020.

[29] Rezazadeh Eidgahee D, Rafiean AH, Haddad A. A Novel Formulation for the Compressive Strength of IBP-Based Geopolymer Stabilized Clayey Soils Using ANN and GMDH-NN Approaches. Iran J Sci Technol Trans Civ Eng 2019. https://doi.org/10.1007/s40996-019-00263-1.

[30] Rezazadeh Eidgahee D, Haddad A, Naderpour H. Evaluation of shear strength parameters of granulated waste rubber using artificial neural networks and group method of data handling. Sci Iran 2019;26:3233–44. https://doi.org/10.24200/sci.2018.5663.1408.

[31] Naderpour H, Rezazadeh Eidgahee D, Fakharian P, Rafiean AH, Kalantari SM. A new proposed approach for moment capacity estimation of ferrocement members using Group Method of Data Handling. Eng Sci Technol an Int J 2020;23:382–91. https://doi.org/10.1016/j.jestch.2019.05.013.

[32] Jahangir H, Rezazadeh Eidgahee D. A new and robust hybrid artificial bee colony algorithm – ANN model for FRP-concrete bond strength evaluation. Compos Struct 2021;257:113160. https://doi.org/10.1016/J.COMPSTRUCT.2020.113160.

[33] Hong J-C, Kim YY, Lee HC, Lee YW. Damage detection using the Lipschitz exponent estimated by the wavelet transform: applications to vibration modes of a beam. Int J Solids Struct 2002;39:1803–16. https://doi.org/10.1016/S0020-7683(01)00279-7.

[34] Chang C-C, Chen L-W. Damage detection of a rectangular plate by spatial wavelet based approach. Appl Acoust 2004;65:819–32. https://doi.org/10.1016/j.apacoust.2004.01.004.

[35] Kim H, Melhem H. Damage detection of structures by wavelet analysis. Eng Struct 2004;26:347–62. https://doi.org/10.1016/j.engstruct.2003.10.008.

[36] Okafor AC, Dutta A. Structural damage detection in beams by wavelet transforms. Smart Mater Struct 2000;9:906–17. https://doi.org/10.1088/0964-1726/9/6/323.

[37] Zhu L-F, Ke L-L, Zhu X-Q, Xiang Y, Wang Y-S. Crack identification of functionally graded beams using continuous wavelet transform. Compos Struct 2019;210:473–85. https://doi.org/10.1016/j.compstruct.2018.11.042.

[38] Xiang J, Liang M. Wavelet-Based Detection of Beam Cracks Using Modal Shape and Frequency Measurements. Comput Civ Infrastruct Eng 2012;27:439–54. https://doi.org/10.1111/j.1467-8667.2012.00760.x.

[39] Xiang J-W, Matsumoto T, Long J-Q, Ma G. Identification of damage locations based on operating deflection shape. Nondestruct Test Eval 2013;28:166–80. https://doi.org/10.1080/10589759.2012.716437.

[40] Xiang J, Liang M, He Y. Experimental investigation of frequency-based multi-damage detection for beams using support vector regression. Eng Fract Mech 2014;131:257–68. https://doi.org/10.1016/j.engfracmech.2014.08.001.

[41] Cao M-S, Xu W, Ren W-X, Ostachowicz W, Sha G-G, Pan L-X. A concept of complex-wavelet modal curvature for detecting multiple cracks in beams under noisy conditions. Mech Syst Signal Process 2016;76–77:555–75. https://doi.org/10.1016/j.ymssp.2016.01.012.

[42] Mirkazemi SB, Jahangir H, Zahmatkesh A. Multiple Damage Identification in Reinforced Concrete Beams via Signal Processing Techniques. 2nd Conf. Urban Planning, Archit. Civ. Eng. Environ., Oslo, Norway: 2021.

[43] Mirkazemi SB, Jahangir H, Zahmatkesh A. Wavelet-Based Time-Domain Damage Localization in RC Beams. 4th Int. Conf. 5th Natl. Conf. Civ. Eng. Archit. Art Urban Des., Tabriz, Iran: 2021.

[44] Jahangir H, Khatibinia M, Kavousi M. Application of Contourlet Transform in Damage Localization and Severity Assessment of Prestressed Concrete Slabs. Soft Comput Civ Eng 2021;5:39–67. https://doi.org/10.22115/SCCE.2021.282138.1301.

[45] Ibrahim D. An Overview of Soft Computing. Procedia Comput Sci 2016;102:34–8. https://doi.org/10.1016/j.procs.2016.09.366.

[46] Mallat S. A wavelet tour of signal processing. London, UK: Academic Press; 1999.

[47] Ovanesova AV, Suárez LE. Applications of wavelet transforms to damage detection in frame structures. Eng Struct 2004;26:39–49. https://doi.org/10.1016/j.engstruct.2003.08.009.

[48] Gao RX, Yan R. Wavelets: Theory and applications for manufacturing. Boston, MA: Springer US; 2011. https://doi.org/10.1007/978-1-4419-1545-0.

[49] Baghiee N, Reza Esfahani M, Moslem K. Studies on damage and FRP strengthening of reinforced concrete beams by vibration monitoring. Eng Struct 2009;31:875–93. https://doi.org/10.1016/j.engstruct.2008.12.009.

[50] Smith M. ABAQUS/Standard User's Manual, Version 6.9. Simulia; 2009.

[51] Misiti M, Misiti Y, Oppenheim G, Poggi JM. Wavelet Toolbox User's Guide. Rev. 4.14. The MathWorks. Inc.; 2014.

[52] Choi S, Park S, Stubbs N. Nondestructive damage detection in structures using changes in compliance. Int J Solids Struct 2005;42:4494–513. https://doi.org/10.1016/j.ijsolstr.2004.12.017.

[53] Harris FJ. On the use of windows for harmonic analysis with the discrete Fourier transform. Proc IEEE 1978;66:51–83. https://doi.org/10.1109/PROC.1978.10837.

[54] Donoho DL, Johnstone IM. Ideal spatial adaptation by wavelet shrinkage. Biometrika 1994;81:425–55. https://doi.org/10.1093/biomet/81.3.425.

[55] Donoho DL. De-noising by soft-thresholding. IEEE Trans Inf Theory 1995;41:613–27. https://doi.org/10.1109/18.382009.